Universiteit Utrecht
Department of Physics and Astronomy
Institute for Theoretical Physics

Master of Science Thesis

Non-spherical Wigner-Seitz cells in linear Poisson-Boltzmann theory

by

Kasimir van Rijn

Supervisor: Dr. R. van Roij

April 24, 2012

Abstract

A common approach to calculate the electrostatic potential in a colloidal crystal is to assume that the neighbor distribution around each colloid is isotropic. In this thesis a numerical model is discussed that keeps the explicit non-isotropic neighbor distribution intact while calculating the electrostatic potential in linear Poisson-Boltzmann theory. The data obtained from this model will be compared with the isotropic approximation and with DLVO theory and it will be shown that at high densities the non-isotropic neighbor distribution cannot be neglected. The model also allows us to investigate an energy dominated fcc/bcc phase transition for varying colloid sizes and predicts that the bcc phase for colloids larger than a certain size becomes inaccessible.

Contents

Chapter 1

Introduction

In 1827 Robert Brown studied pollen grains under his light microscope and observed that micron-sized objects on a water-air interface display random movement, which is nowadays known as Brownian-motion. This phenomenon was, as explained by Einstein in one of his three famous papers in 1905, caused by collisions with molecules that are exhibiting thermal movement. Einstein was able to determine the diffusion of these particles in terms of their size, the temperature and the viscosity of the solvent. The particles that Brown observed are an example of a class of particles called colloids. The class of colloids consist of particles in a liquid or gas that have sizes between 10 nm and 1 μm. Colloids are large compared to the solvent molecules and so the solvent can be approximated as a continuum, while at the same time the colloids are small enough to move noticeably due to collisions with small solvent molecules, which means that they perform Brownian-motion. Examples of colloids are paints, inks, cosmetic products and all kinds of food products which consist of colloidal particles suspended in a liquid continuous medium [1], e.g. mayonnaise and yogurt. This means that there is a lot of industrial interest for colloid studies. Another reason why colloids are interesting to study is because their thermodynamic properties are similar to those of atomic and molecular systems. Because the size of the colloids is larger and the time scale in colloidal systems is larger it is much easier to observe colloids than atoms or molecules. Also, with the progress in chemical synthesis in the last decades colloids can be made in all kinds of shapes and have all sorts of properties, for instance they can be made into dumbbells, cubes or caps [1]. The interest in colloidal systems thus has a practical and a fundamental origin and for these reasons there is still a lot of research done on these kind of systems.

1.1 Charged colloids and DLVO theory

When a colloid is suspended in a (monovalent) ionic solution it might happen that the colloid gains a net surface charge by either adsorption or dissociation of a particular ion of the solvent. For example, when AgCl colloids are suspended in a chloride solution they can absorb the Cl^- ions of the ionic solution or when suspended in a silver ion solution they will absorb the Ag^+ ions. In either case the AgCl colloids gain a net surface charge. Another example is when one suspends a soap Na(RCOO), with R an organic group, in water. In this case the Na^+ ions dissociate form the $(ROO)^-$ groups. The $(ROO)^-$ groups cluster together to form a negatively charged colloid.

The surface charge of a colloid causes ions of opposite charge to surround the colloid and a so called "double layer" is formed. The effect of this double layer is that it screens the charge of the colloid, such that at a large distance (a couple of screening lengths) the colloid seems to be charge neutral. The typical size of such a double layer is characterized by the Debye length of the electrolyte $1/\kappa$. In the 1940s Derjaguin and Landau and Verwey and Overbeek independently calculated the effective potential for two homogeneously charged colloidal spheres. This potential consisted of an attractive Van der Waals potential ($\sim r^{-6}$) and a repulsive Yukawa potential ($\sim e^{-\kappa r}/r$). Since the Van der Waals potential is often scaled away by making sure that the colloids and the solvent have (almost) the same refractive index (called "index matching") [2], it is usual to study only the Yukawa part of this potential [3], which we will refer to as DLVO potential. In this thesis we will also only study the repulsive DLVO potential, although we must acknowledge that at the very short distance we will consider one cannot always ignore the Van der Waals force.

It is possible to determine the properties of a suspension of charged colloids by making use of the Poisson-Boltzmann equation to find the electric potential inside the solvent, such that, for example, the ionic densities in the solvent can be calculated. A common approach is to introduce Wigner-Seitz cells (see chapter 2) around each colloid and use a spherical approximation for these cells to greatly simplify the calculations to find the solution of the Poisson-Boltzmann equation. When making this approximation, however, one automatically assumes that the electric potential on the colloid's surface (zeta-potential) is uniform. Although this might lead in some cases to quantitative agreement with experiments, it is the case that some experiments cannot be explained by making this assumption [4]. The aim of this thesis is to explore the effect of allowing non-uniform zeta potentials for colloids in crystal structures. We will study only the face centered cubic (fcc) and the body centered cubic (bcc) crystal structures in linear Poisson-Boltzmann theory. The reason for doing only linear theory is that, to our knowledge, not much is written in the literature about Poisson-Boltzmann theory for non-spherical Wigner-Seitz cells. This means

that the effect of having a non-uniform zeta potential might as well be neglected and so no extra effort has to be done to create numerical methods for non-linear Poisson-Boltzmann theory. It is important to note that only recently experimental techniques, such as atomic force microscopy, were developed that allow measurement on non-uniform surface potentials on colloids [4], which might also be the reason for the limited amount of literature on this subject. Also, since we are making use of an approximate numerical method for computing the potential in the non-uniform case, it is useful to compare our results with the known results in linear theory, such as DLVO theory. One could say that this thesis is a exploration which establishes if further research in this direction can be well rewarded.

1.2 Outline

Before looking at the non-spherical Wigner-Seitz cells it is good to review some general thermodynamics and derive the repulsive part of DLVO theory, this is done in the first part of chapter 2. We will derive DLVO theory in two different ways, one following a density functional approach as in Ref. [3], and one following a more physical intuitive approach as in Ref. [1]. The next part of chapter 2 consist of the application of DLVO theory to colloidal fcc and bcc crystals. We will introduce a dimensionless parameter which measures the fcc/bcc phase transition in the point particle limit. This will be a guide for testing our model which solves the Poisson-Boltzmann equation for non-spherical Wigner- Seitz cells. This model is described in chapter 3. In chapter 4 we present the data obtained form numerical calculations from the model discussed in chapter 3. Here we will check that the model satisfies the minimal qualitative expectations one can formulate on physical ground. Subsequently we will investigate the magnitude of the colloid's surface heterogeneous potential distribution is and compare it with the results for a uniform zeta potential (spherical Wigner-Seitz cell approximation). Then we will compare our results with DLVO theory and try to obtain the correct critical value for the parameter which measures the phase transition fcc/bcc. Finally we will look at the effect of different dielectric ratios between the solvent and the colloid on the energy of the system.

Chapter 2

Theoretical Background

In this chapter the theoretical background for the model under consideration will be discussed. The first section deals with general statistical physics and DLVO theory, while the second section discusses crystal structures and the application of DLVO theory to them. This chapter is meant to be self-contained, but in some instances a reference to more in-depth literature will be given.

2.1 Statistical physics and DLVO-theory

For the purpose of understanding the behavior of charged colloids suspended in a molecular solvent with monovalent cations and anions, it is appropriate to use the language and tools of statistical physics. For that reason the canonical and the grand canonical ensembles are discussed together with classical density functional theory (DFT). The theory is applied to the ideal gas as a simple example. Subsequently the Poisson-Boltzmann (PB) equation will be derived and two derivations will be given of DLVO-theory: one which follows a grand-canonical approach as in Ref. [3] and an other in which a more physical picture is presented as in Ref. [1]. From this physical picture some of the drawbacks of DLVO theory are made clear.

2.1.1 Classical ensemble theory

Here a short overview of classical ensemble theory is given based on Ref. [5], which should be consulted for a more detailed discussion on the subject.

In order to describe a closed system of N identical particles in a three dimensional volume V, where each particle has three translational degrees of freedom, we must specify the phase point $\Gamma(\mathbf{r}^N, \mathbf{p}^N)$ in the $6N$-dimensional phase space. Here $\mathbf{r}^N = \{\mathbf{r}_1, ..., \mathbf{r}_N\}$ are the three dimensional coordinates of the particles and

$\mathbf{p}^N = \{\mathbf{p}_1, ..., \mathbf{p}_N\}$ are the conjugate momenta. An *ensemble* is a large collection of such systems, which only differ by their position in phase space. If a probability density $f(\Gamma, t)$ is given which characterizes the ensemble at time t by a cloud of phase points distributed accordingly to this density, then the time evolution of $f(\Gamma, t)$ is given by Liouville's theorem:

$$\frac{\partial f(\Gamma, t)}{\partial t} = \{H, f\}, \tag{2.1}$$

where $\{,\}$ are the usual Poisson brackets and H is the Hamiltonian of the system. In equilibrium statistical mechanics the probability density is stationary, i.e. $\frac{\partial f(\Gamma,t)}{\partial t} = 0$, which implies by virtue of (2.1) that $f(\Gamma, t)$ must be expressible in terms of conserved quantities, such as the energy.

There are different kinds of ensembles which can describe physical system, but the must useful ones are the micro canonical, canonical and grand canonical ensembles. The micro canonical ensemble consists of a closed system with a fixed number of particles, volume and energy. In the canonical ensemble the system is connected with a heat bath or reservoir, such that energy exchange is possible, but the volume and number of particles is still fixed. Statistical equilibrium is reached when the temperature of the system equals that of the reservoir. In the grand canonical ensemble it is, next to energy transfer, also possible to exchange particles with the reservoir, which leads to the introduction of a chemical potential μ that determines the equilibrium of particle exchange, i.e. the chemical potential of the system must become equal to the chemical potential of the reservoir by particle transfer. Each of these descriptions has its own normalized probability density, which can be found by making use of partition functions. The partition function links the microscopic description of the system to the macroscopic observable quantities by summing (or integrating) over all states of the system with an appropriate weight. We will now give these partition functions for the canonical and grand canonical ensembles and work out some of their properties.

Canonical ensemble

In the canonical ensemble the system can exchange energy with a (much larger) reservoir, which leads to the well known Boltzmann weight factors. The canonical partition function for the canonical ensemble with volume V, number of (identical) particles N and temperature T is given by

$$Z(N, V, T) = \frac{1}{N! h^{3N}} \int d\Gamma \exp[-\beta H(\Gamma)], \tag{2.2}$$

where h is Planck's constant, β is the inverse thermal energy and $H(\Gamma)$ is the Hamiltonian of the system corresponding to the phase point Γ. This directly gives us the

probability density function

$$f_c(\Gamma) = \frac{\exp[-\beta H(\Gamma)]}{N! h^{3N} Z(N,V,T)}, \tag{2.3}$$

where the subscript c stands for canonical ensemble. The average energy of the system can be found by integrating the weighted Hamiltonian over all of phase space:

$$\begin{aligned}\langle E\rangle &= \int d\Gamma H(\Gamma) f_c(\Gamma) \\ &= \frac{1}{N! h^{3N} Z(N,V,T)} \int d\Gamma H(\Gamma) \exp[-\beta H(\Gamma)] \\ &= \frac{1}{N! h^{3N} Z(N,V,T)} \frac{-\partial}{\partial\beta} \int d\Gamma \exp[-\beta H(\Gamma)] \\ &= \frac{-\partial \log[Z(N,V,T)]}{\partial\beta}.\end{aligned} \tag{2.4}$$

Also the average entropy can be found in a similar way

$$\begin{aligned}\langle S\rangle &= -k_B \int d\Gamma f_c(\Gamma) \log[f_c(\Gamma) N! h^{3N}] \\ &= \frac{-k_B}{N! h^{3N} Z(N,V,T)} \int d\Gamma \exp[-\beta H(\Gamma)] \log\Big[\frac{\exp[-\beta H(\Gamma)]}{Z(N,V,T)}\Big] \\ &= \frac{k_B}{N! h^{3N} Z(N,V,T)} \int d\Gamma \beta H(\Gamma) \exp[-\beta H(\Gamma)] \\ &- \frac{-k_B \log[Z(N,V,T)]}{N! h^{3N} Z(N,V,T)} \int d\Gamma \exp[-\beta H(\Gamma)] \\ &= \frac{1}{T}\langle E\rangle + \frac{k_B T}{T} \log[Z(N,V,T)],\end{aligned} \tag{2.5}$$

where we used the phase space density $N! h^{3N}$ to make the argument of the logarithm is dimensionless. The factor $N!$ is the number of indistinguishable configurations for identical particles.

By defining the Helmholtz free energy $F(N,V,T) \equiv -k_B T \log[Z(N,V,T)]$, it follows from equations (2.4) and (2.5) that $F(N,V,T) = \langle E\rangle - \langle S\rangle T$ and hence it is constant in the canonical ensemble for fixed N and V. It is possible to calculate other physical quantities by taking partial derivatives of the free energy, for instance the pressure p and chemical potential μ of the system are given by

$$p = -\Big(\frac{\partial F(N,V,T)}{\partial V}\Big)_{N,T}, \qquad \mu = \Big(\frac{\partial F(N,V,T)}{\partial N}\Big)_{V,T}. \tag{2.6}$$

Grand canonical ensemble

In addition to the exchange of energy, which is possible in the canonical ensemble, it is also possible to transfer particles between the reservoir and the system in the

grand canonical ensemble. This leads to the introduction of a chemical potential μ of the system which basically regulates the particle exchange. The grand canonical partition function for fixed μ, V and T is given by

$$\begin{aligned}\Xi(\mu, V, T) &= \sum_{N=0}^{\infty} \frac{\exp[\beta\mu N]}{N!h^{3N}} \int d\Gamma \exp[-\beta H(\Gamma)] \\ &= \sum_{N=0}^{\infty} \exp[\beta\mu N] Z(N, V, T). \end{aligned} \tag{2.7}$$

The corresponding probability density function (with subscript g for grand canonical) is

$$f_g(\Gamma, N) = \frac{\exp[-\beta H(\Gamma) + \beta\mu N]}{N!h^{3N}\Xi(\mu, V, T)}. \tag{2.8}$$

The average energy and entropy of the system can be found in a similar way as in the canonical setting. A different interesting quantity that can now be calculated is the average number of particles $\langle N \rangle$. It is given by

$$\begin{aligned}\langle N \rangle &= \sum_{N=0}^{\infty} \int d\Gamma N f_g(\Gamma, N) \\ &= \sum_{N=0}^{\infty} \frac{N exp[\beta\mu N]}{N!h^{3N}\Xi(\mu, V, T)} \int d\Gamma exp[-\beta H(\Gamma)] \\ &= \sum_{N=0}^{\infty} \frac{N exp[\beta\mu N] Z(N, V, T)}{\Xi(\mu, V, T)} \\ &= \frac{\partial}{\partial\beta\mu} \log[\Xi(\mu, V, T)]. \end{aligned} \tag{2.9}$$

This leads to the definition of the grand potential $\Omega(\mu, V, T) \equiv -k_B T \log[\Xi(\mu, V, T)]$, which is constant for the grand canonical ensemble and can be shown to be equal to

$$\Omega(\mu, V, T) = \langle E \rangle - \langle S \rangle T - \mu\langle N \rangle = F - \mu\langle N \rangle. \tag{2.10}$$

The ideal gas

A simple, but useful application of the above can be given to a system of N non-interacting particles in a volume V at temperature T, also known as an ideal gas. In this case the Hamiltonian of the system only contains the kinetic energy of the particles and can be written as $H = \sum_{i=0}^{N} \frac{\mathbf{p}_i^2}{2m}$. In the canonical ensemble we find by doing a Gaussian integration

$$Z(N, V, T) = \frac{1}{N!h^{3N}} \prod_{i=0}^{N} \iint d\mathbf{r}_i d\mathbf{p}_i \exp\Big[-\frac{\beta\mathbf{p}_i^2}{2m}\Big] = \frac{V^N}{N!\Lambda^{3N}}, \tag{2.11}$$

where $\Lambda = \frac{h}{\sqrt{2\pi m k_B T}}$ is the thermal (De Broglie) wave length. Having obtained the expression for the partition function it is now easy to compute the free energy with use of the Stirling approximation $\log N! = N \log N - N$:

$$F = -k_B T \log[Z] = -k_B T \log\Big[\frac{V^N}{N!\Lambda^{3N}}\Big] \approx N k_B T \Big(\log\Big[\frac{N\Lambda^3}{V}\Big] - 1\Big). \quad (2.12)$$

From this the chemical potential can be computed, which will be used later on. The chemical potential is given by

$$\mu = \Big(\frac{\partial F(N,V,T)}{\partial N}\Big)_{V,T} = k_B T \log\Big[\frac{N\Lambda^3}{V}\Big]. \quad (2.13)$$

2.1.2 Classical density functional theory

In order to derive the PB equation and the DLVO potential it is appropriate to briefly introduce the subject of classical DFT. Classical DFT is a method of statistical physics where one uses functionals and correlation functions to determine the properties of the system of interest. The main ingredients are the one-particle density $\rho(\mathbf{r})$ and the free energy functional $\mathcal{F}[\rho(\mathbf{r})]$. An example of a one-particle density function is for instance the distribution of positive or negative ions in a solution. The free energy functional must then be written in terms of these densities, such that minimizing methods can be applied to find the equilibrium density. A short summary of the main properties of density functional theory will now be given as in Ref. [6]. For a more detailed treatment of the subject consult Ref. [5].

Consider a system of volume V in contact with a particle and heat reservoir with chemical potential μ and temperature T. Furthermore suppose that the system is under influence of an external potential $V_{\text{ext}}(\mathbf{r})$. If the positions of the particles are denoted by $\mathbf{r}_i$, then the one particle density $\rho(\mathbf{r})$ is given as the ensemble average

$$\rho(\mathbf{r}) = \Big\langle \sum_i \delta(\mathbf{r} - \mathbf{r}_i) \Big\rangle. \quad (2.14)$$

As is shown in Ref. [5], a $V_{\text{ext}}(\mathbf{r})$ gives rise to a unique $\rho(\mathbf{r})$ and an equilibrium one-particle density $\rho_0(\mathbf{r})$ gives rise to a unique $V_{\text{ext}}(\mathbf{r})$. As mentioned in the previous section (Eq. (2.10)), all physical properties can be derived from the grand potential of the system, which is now a functional $\Omega = \Omega[\rho_0(\mathbf{r})]$ of the equilibrium one-particle density. It can be written as

$$\Omega[\rho_0(\mathbf{r})] = \mathcal{F}[\rho_0(\mathbf{r})] + \int d\mathbf{r} \rho_0(\mathbf{r})(V_{\text{ext}}(\mathbf{r}) - \mu). \quad (2.15)$$

The remarkable property of this functional approach is that when one allows in the grand potential functional any other one-particle density $\rho(\mathbf{r})$ different from the equilibrium density, it has the following property:

$$\Omega[\rho_0(\mathbf{r})] \leq \Omega[\rho(\mathbf{r})]. \quad (2.16)$$

This means that the equilibrium density minimizes the grand potential functional and can thus be computed by one of the following equations (Euler-Lagrange equations),

$$\frac{\delta\Omega[\rho(\mathbf{r})]}{\delta\rho(\mathbf{r})}\Big|_{\rho=\rho_0} = 0, \qquad \frac{\delta\mathcal{F}[\rho(\mathbf{r})]}{\delta\rho(\mathbf{r})}\Big|_{\rho=\rho_0} + V_{\text{ext}}(\mathbf{r}) - \mu = 0, \tag{2.17}$$

where functional derivatives are taken.

Example: the ideal gas

The free energy functional can be split into a ideal $\mathcal{F}_{\text{id}}[\rho(\mathbf{r})]$ part and an excess part $\mathcal{F}_{\text{ex}}[\rho(\mathbf{r})]$, such that $\mathcal{F}[\rho(\mathbf{r})] = \mathcal{F}_{\text{id}}[\rho(\mathbf{r})] + \mathcal{F}_{\text{ex}}[\rho(\mathbf{r})]$. The free energy functional for an ideal gas is given by

$$\beta\mathcal{F}_{\text{id}}[\rho(\mathbf{r})] = \int d\mathbf{r}\rho(\mathbf{r})(\log(\rho(\mathbf{r})\Lambda^3) - 1). \tag{2.18}$$

Assuming that there is no external potential, the grand potential functional becomes with use of equations (2.13) and (2.15)

$$\beta\Omega_{\text{id}}[\rho(\mathbf{r})] = \int d\mathbf{r}\rho(\mathbf{r})(\log\left(\frac{\rho(\mathbf{r})}{\rho_s}\right) - 1), \tag{2.19}$$

where the bulk density $\rho_s = \frac{N}{V}$ that satisfies $\mu = k_B T \log[\rho_s\Lambda^3]$ was introduced.

2.1.3 Colloids in a salty suspension

In this section the model that forms the basis for the remainder of this thesis will be described together with its characterizing functionals and densities. We will consider a suspension of N colloids of radius a and charge Ze, where e is the elementary charge, in a solvent which also contains monovalent salt ions (i.e. of charge $\pm e$) and is connected with a reservoir with which the system can exchange salt ions and energy. The reservoir is at temperature T and has a chemical potential μ_+ for cations $(+)$ and μ_- for anions $(-)$. The colloids cannot enter the reservoir and are at positions $\{\mathbf{R}_i\}$, where $i = 1, ..., N$. As is usual in physical models some approximations have to be made in order to simplify the calculations. A schematic overview of these approximations are given in Fig. 2.1. In Fig. 2.1(a) the microscopic model is depicted. In this description interactions between colloids, positive and negative ions and the solvent molecules must be taken into account. The first approximation is to consider the solvent as a continuous background which can be characterized by a dielectric constant ϵ, see Fig. 2.1(b). The second approximation is to use a density profile $\rho_\pm(\mathbf{r})$ for the salt ions, such that the DFT framework becomes applicable, see Fig. 2.1(c). The ion concentration in the reservoir is considered to be a bulk concentration ρ_s. The interactions that need to be taken into account are the colloid-colloid, colloid-ion and ion-ion Coulomb interactions. Hard-core interactions between the colloids will also be taken into account. This means that colloids cannot overlap

and ions cannot penetrate the colloids. The treatment given below, including the derivation of the PB-equation and the DFT approach to DLVO theory is based on Ref. [3].

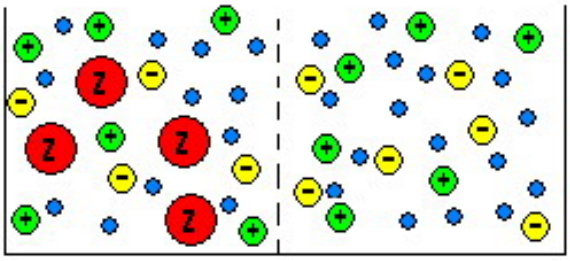

(a) Microscopic model, take into account interactions between the colloids, ions and solvent molecules.

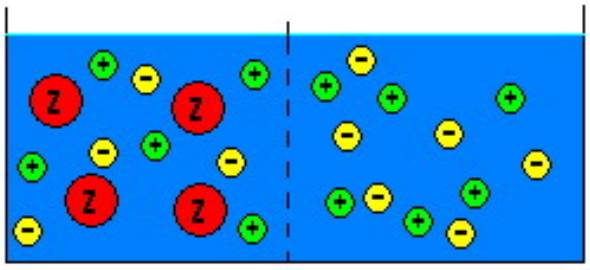

(b) Continuous background model, characterize the solvent by a dielectric constant ϵ.

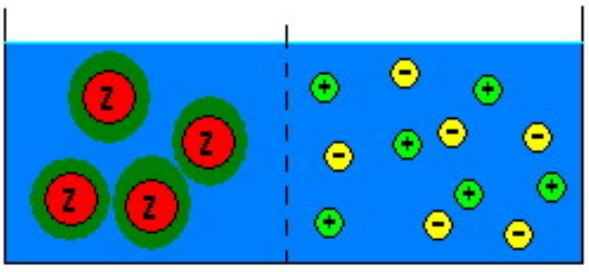

(c) Effective density model, introduce a density profile $\rho_{\pm}(\mathbf{r})$ for the ions. The ion density in the reservoir is taken equal to the constant ρ_s.

Figure 2.1: Graphical impression of the different levels of approximation for the colloidal suspension. Here the colloids are red, positive ions green, negative ions yellow and solvent molecules blue. These figures are not on scale.

Define the following potential, which takes into account the hard-core and Coulomb

interactions between the ions and the colloids,

$$\beta V_{c\pm}(r) = \begin{cases} \infty, & r < a \\ \mp \frac{Z\lambda_B}{r}, & r > a, \end{cases} \tag{2.20}$$

where the Bjerrum length $\lambda_B = \frac{e^2}{\epsilon k_B T}$ was used. In the mean field approximation of density profiles $\rho_\pm(\mathbf{r})$ for the ion concentration, define the external potentials $U_\pm(\mathbf{r}) = \sum_{i=1}^{N} V_{c\pm}(|\mathbf{R}_i - \mathbf{r}|)$. Taking a fixed colloid configuration $\{\mathbf{R}_i\}$ and introducing the total density $\rho(\mathbf{r}) = \rho_+(\mathbf{r}) - \rho_-(\mathbf{r})$, the grand-canonical potential functional for the ions can be written as

$$\begin{aligned} \Omega[\rho_+, \rho_-] = \Omega_{id}[\rho_+] + \Omega_{id}[\rho_-] + \frac{e^2}{2\epsilon} \int d\mathbf{r} d\mathbf{r}' \frac{\rho(\mathbf{r})\rho(\mathbf{r}')}{|\mathbf{r} - \mathbf{r}'|} \\ + \int d\mathbf{r} \Big(\rho_+(\mathbf{r}) U_+(\mathbf{r}) + \rho_-(\mathbf{r}) U_-(\mathbf{r}) \Big). \end{aligned} \tag{2.21}$$

The terms $\Omega_{id}[\rho_\pm]$ are the ideal-gas functionals, defined in equation (2.19).

2.1.4 The Poisson-Boltzmann equation and linear approximation

It is useful to define the dimensionless electrostatic potential by

$$\phi(\mathbf{r}) = \lambda_B \int d\mathbf{r}' \frac{\rho(\mathbf{r}') + q(\mathbf{r}')}{|\mathbf{r} - \mathbf{r}'|}, \tag{2.22}$$

where $q(\mathbf{r}) = \sum_{i=1}^{N} \frac{Z}{4\pi a^2} \delta(|\mathbf{r} - \mathbf{R}_i| - a)$ is the colloidal charge term. Working out the Euler-Lagrange equations (2.17) for the functional (2.21) outside the hard-cores gives

$$\begin{aligned} \frac{\delta\Omega[\rho_+, \rho_-]}{\delta\rho_\pm(\mathbf{r})} = \beta \frac{\delta\Omega_{id}[\rho_\pm]}{\delta\rho_\pm(\mathbf{r})} \pm \phi(\mathbf{r}) = 0 \\ \Rightarrow \ln\left(\frac{\rho_\pm(\mathbf{r})}{\rho_s}\right) \pm \phi(\mathbf{r}) = 0 \\ \Rightarrow \rho_\pm(\mathbf{r}) = \rho_s \exp[\mp\phi(\mathbf{r})]. \end{aligned} \tag{2.23}$$

Now using the Poisson equation, which is equivalent to equation (2.22), together with the Boltzmann distribution (2.23) the PB-equation is obtained,

$$\begin{aligned} \nabla^2\phi(\mathbf{r}) &= -4\pi\lambda_B(\rho(\mathbf{r}) + q(\mathbf{r})) \\ &= \kappa^2 \sinh(\phi(\mathbf{r})) - \frac{Z\lambda_B}{a^2} \sum_{i=1}^{N} \delta(|\mathbf{r} - \mathbf{R}_i| - a), \end{aligned} \tag{2.24}$$

where the Debye length κ^{-1} was introduced by $\kappa^2 = 8\pi\lambda_B\rho_s$.

The problem at hand is to find a solution to this multi-centered non-linear differential equation for $\phi(\mathbf{r})$. With this solution the equilibrium density profiles $\rho_\pm(\mathbf{r})$ can

be obtained by (2.23) and thus the equilibrium grand-potential functional (2.21) is then found. Including in this grand-potential the colloid-colloid interactions solves the model. Unfortunately there are no analytical solutions known to the multi-centered non-linear PB-equation and it is also hard to solve it numerically. Therefore some more approximations must be made. The assumption we make is that the ion-densities $\rho_\pm(\mathbf{r})$ are only small deviations (up to second order) of the average densities $\bar{\rho}_\pm$ given by $\int d\mathbf{r}(\rho_\pm(\mathbf{r}) - \bar{\rho}_\pm) = 0$. The exact expressions for this average densities in terms of system parameters will be calculated later on. Using this expansion gives an approximation for the ideal-gas functional $\Omega_{id}[\rho_\pm] \approx \Omega'_{id}[\rho_\pm]$, where the approximate ideal-gas functional is given by

$$\begin{aligned}\beta\Omega'_{id}[\rho_\pm] = \bar{\rho}_\pm(\ln\frac{\bar{\rho}_\pm}{\rho_s} - 1)V + \ln\frac{\bar{\rho}_\pm}{\rho_s}\int d\mathbf{r}(\rho_\pm(\mathbf{r}) - \bar{\rho}_\pm) \\ + \frac{1}{2\bar{\rho}_\pm}\int d\mathbf{r}(\rho_\pm(\mathbf{r}) - \bar{\rho}_\pm)^2. \end{aligned} \tag{2.25}$$

The final approximation is to write the potentials $U_\pm(\mathbf{r})$ in terms of two new potentials $V(\mathbf{r}) = \sum_{i=1}^N v(|\mathbf{r} - \mathbf{R}_i|)$ and $W(\mathbf{r}) = \sum_{i=1}^N w(|\mathbf{r} - \mathbf{R}_i|)$ which are defined by the following pair potentials

$$\beta v(r) = \begin{cases} \beta v_0, & r < a \\ -\frac{Z\lambda_B}{r}, & r > a \end{cases}, \tag{2.26}$$

$$\beta w(r) = \begin{cases} \beta w_0, & r < a \\ 0, & r > a \end{cases}, \tag{2.27}$$

where the two hard-core parameters v_0 and w_0 will be determined in such a way that the ion-densities of both species vanishes inside the colloids. Now let $U_\pm(\mathbf{r}) = \pm V(\mathbf{r}) + \frac{2\bar{\rho}_\pm}{\bar{\rho}_+ + \bar{\rho}_-}W(\mathbf{r})$, such that the grand-potential functional (2.21) becomes

$$\begin{aligned}\Omega[\rho_+, \rho_-] = \Omega'_{id}[\rho_+] + \Omega'_{id}[\rho_-] + \frac{e^2}{2\epsilon}\int d\mathbf{r}d\mathbf{r}'\frac{\rho(\mathbf{r})\rho(\mathbf{r}')}{|\mathbf{r} - \mathbf{r}'|} \\ + \int d\mathbf{r}\Big(\rho(\mathbf{r})V(\mathbf{r}) + (\rho_+(\mathbf{r}) + \rho_-(\mathbf{r}))W(\mathbf{r})\Big). \end{aligned} \tag{2.28}$$

By introducing a new dimensionless electrostatic potential

$$\phi(\mathbf{r}) = \lambda_B\int d\mathbf{r}'\frac{\rho(\mathbf{r}')}{|\mathbf{r} - \mathbf{r}'|} + \beta V(\mathbf{r}), \tag{2.29}$$

the Euler-Lagrange equations (2.17) for the approximate grand-potential (2.28) become

$$\ln\frac{\bar{\rho}_\pm}{\rho_s} + \frac{\rho_\pm(\mathbf{r}) - \bar{\rho}_\pm}{\bar{\rho}_\pm} \pm \phi(\mathbf{r}) + \frac{2\bar{\rho}_\pm\beta W(\mathbf{r})}{\bar{\rho}_+ + \bar{\rho}_-} = 0. \tag{2.30}$$

Due to the approximations, the densities $\rho_\pm(\mathbf{r})$ are now linear in the electrostatic potential $\phi(\mathbf{r})$, such that, combined with the Poisson equation, the PB-equation has

now been linearized. The exact expression is not important, since it is expressed in $\bar{\rho}_\pm$, which still need to be determined in terms of system parameters. Later on the linear PB-equation that will be used for numerical calculations is obtained by simply expanding (2.24) around zero average potential. One can check that both methods lead to the same result, see Ref. [7].

Introduce the following two quantities, the packing fraction $\eta = V_{\text{colloids}}/V$, where V_{colloids} is the total volume taken by the colloids, and the Donnan potential $\bar{\phi} = \frac{1}{V}\int d\mathbf{r}\phi(\mathbf{r})$. The average densities $\bar{\rho}_\pm$ are obtained in terms of system parameters by integrating (2.30) over the total volume of the system. One obtains the following expression

$$\bar{\rho}_\pm = \rho_s \exp\Big[\mp\bar{\phi} - \frac{2\bar{\rho}_\pm\beta\eta w_0}{\bar{\rho}_+ + \bar{\rho}_-}\Big], \tag{2.31}$$

here the hard-core parameter w_0 still needs to be determined. Using charge neutrality of the system $\bar{\rho}_+ - \bar{\rho}_- = Zn$ gives the Donnan potential in terms of system parameters

$$\bar{\phi} = -\sinh^{-1}\Big[\frac{Zn}{2\rho_s}e^{\beta w_0\eta}\Big] + \frac{Zn}{\bar{\rho}_+ + \bar{\rho}_-}\beta w_0\eta, \tag{2.32}$$

such that after some algebraic steps one finally obtains

$$\bar{\rho}_\pm = \frac{1}{2}\Big(\sqrt{(Zn)^2 + (2\rho_s)^2 e^{-2\beta w_0\eta}} \pm Zn\Big). \tag{2.33}$$

Now that exact expressions for the average ion-densities have been obtained, the Euler-Lagrange equations (2.30) need to be solved in order to fix the hard-core parameters v_0 and w_0. The solution of the EL-equations will give the grand potential (2.28) the expected DLVO-form.

2.1.5 DLVO-theory: A DFT approach

Consider the following two linear combinations of the EL-equations (2.30),

$$\frac{\rho_+(\mathbf{r})}{\bar{\rho}_+} + \frac{\rho_-(\mathbf{r})}{\bar{\rho}_-} = 2(1 - \beta W(\mathbf{r}) + \eta\beta w_0), \tag{2.34}$$

$$\frac{\rho(\mathbf{r}) - \bar{\rho}}{\bar{\rho}_+ + \bar{\rho}_-} = -(\phi(\mathbf{r}) - \bar{\phi}), \tag{2.35}$$

where $\bar{\rho} = \bar{\rho}_+ - \bar{\rho}_-$. To ensure that the ion-density inside the colloids is zero, impose the condition $\frac{\rho_+(\mathbf{r})}{\bar{\rho}_+} + \frac{\rho_-(\mathbf{r})}{\bar{\rho}_-} = 0$ inside the colloids. Combining this relation with (2.34) gives an expression for the hard-core parameter, $\beta w_0 = \frac{1}{1-\eta}$. Using this in expression (2.34) gives, for outside the colloids, $\frac{\rho_+(\mathbf{r})}{\bar{\rho}_+} + \frac{\rho_-(\mathbf{r})}{\bar{\rho}_-} = \frac{2}{1-\eta}$. Equation (2.34) is now solved and by doing so an expression for βw_0 in terms of system parameters was obtained, which completely fixes the Donnan potential and the average ion-densities.

To solve the second Euler-Lagrange equation (2.35), define the Fourier transform of a function $f(\mathbf{r})$ by $f_{\mathbf{k}} = \int d\mathbf{r} f(\mathbf{r}) e^{i\mathbf{k}\cdot\mathbf{r}}$. To ensure that $\rho(\mathbf{r})$ will be a multi-centered sum of DLVO profiles, fix the hard-core parameter v_0 to $\beta v_0 = -Z\frac{\bar{\kappa}\lambda_B}{1+\bar{\kappa}a}$, where $\bar{\kappa}^2 = 4\pi\lambda_B(\bar{\rho}_+ + \bar{\rho}_-)$. Taking the Fourier transform of (2.35) gives

$$\rho_{\mathbf{k}} = (2\pi)^3\Big((\bar{\rho}_+ + \bar{\rho}_-)\bar{\phi} + \bar{\rho}\Big)\delta(\mathbf{k}) - (\bar{\rho}_+ + \bar{\rho}_-)\phi_{\mathbf{k}}. \tag{2.36}$$

Now by using some standard Fourier transforms determine $\phi_{\mathbf{k}}$ by taking the transform of equation (2.29), this leads to

$$\begin{aligned}\phi_{\mathbf{k}} &= 4\pi\lambda_B\frac{\rho_{\mathbf{k}}}{k^2} \\ &\quad - \frac{4\pi a}{k^2}\sum_{j=1}^{N}\exp[i\mathbf{k}\cdot\mathbf{R}_j]\Big\{\big(Z\frac{\lambda_B}{a} - Z\frac{\bar{\kappa}\lambda_B}{1+\bar{\kappa}a}\big)\cos ka + Z\frac{\bar{\kappa}\lambda_B}{1+\bar{\kappa}a}\frac{\sin ka}{ka}\Big\}.\end{aligned} \tag{2.37}$$

Solving the linear system of equations (2.36) and (2.37) finally gives

$$\begin{aligned}\rho_{\mathbf{k}} &= (2\pi)^3\big\{(\bar{\rho}_+ + \bar{\rho}_-)\bar{\phi}\big\}\frac{k^2}{k^2+\bar{\kappa}^2}\delta(\mathbf{k}) \\ &\quad + \frac{Z}{1+\bar{\kappa}a}\frac{\cos ka + \frac{\bar{\kappa}}{k}\sin ka}{1+\frac{k^2}{\bar{\kappa}^2}}\sum_{j=1}^{N}\exp[i\mathbf{k}\cdot\mathbf{R}_j].\end{aligned} \tag{2.38}$$

Now by transforming (2.38) back to real space, the density profiles are given by a multi-centered sum $\rho(\mathbf{r}) = \sum_{i=1}^{N}\rho_1(|\mathbf{r}-\mathbf{R}_i|)$, where the individual profiles are given by the usual DLVO form

$$\rho_1(r) = \begin{cases} 0, & r < a \\ \dfrac{Z\bar{\kappa}^2}{4\pi}\dfrac{\exp[\bar{\kappa}a]}{1+\bar{\kappa}a}\dfrac{\exp[-\bar{\kappa}r]}{r}, & r > a. \end{cases} \tag{2.39}$$

Collecting the solutions for the Euler-Lagrange equations (2.34) and (2.35), solving for $\rho_\pm(\mathbf{r})$ and substituting these expressions back in the grand-potential functional (2.28), the last term vanishes and what remains is

$$\frac{\beta\Omega}{V} = \sum_{i=\pm}\bar{\rho}_i\big(\ln\frac{\bar{\rho}_i}{\rho_s} - 1\big) + \frac{Zn}{2} + \frac{\eta}{1-\eta}\frac{2\bar{\rho}_+\bar{\rho}_-}{\bar{\rho}_+ + \bar{\rho}_-} + \frac{1}{2V}\int d\mathbf{r}\rho(\mathbf{r})\beta V(\mathbf{r}). \tag{2.40}$$

Now to compute the integral, use Parseval's theorem, $\int d\mathbf{r}\rho(\mathbf{r})\beta V(\mathbf{r}) = \int d\mathbf{k}\rho_{\mathbf{k}}\beta V_{\mathbf{k}}$, to arrive at

$$\begin{aligned}\frac{1}{2V}\int d\mathbf{r}\rho(\mathbf{r})\beta V(\mathbf{r}) &= \frac{1}{V}\sum_{i<j}\left\{\left(\frac{Ze^{\bar{\kappa}a}}{1+\bar{\kappa}a}\right)^2\frac{\lambda_B e^{-\bar{\kappa}R_{ij}}}{R_{ij}} - Z^2\frac{\lambda_B}{R_{ij}}\right\} \\ &\quad - \frac{n}{2}\frac{Z^2\bar{\kappa}\lambda_B}{1+\bar{\kappa}a} - \frac{1}{2}\frac{(\rho_+ - \bar{\rho}_-)^2}{\rho_+ + \bar{\rho}_-} - \frac{Zn}{2}\bar{\phi}.\end{aligned} \tag{2.41}$$

Putting it all together gives the final form of the grand-potential

$$\beta\Omega = \left(\frac{Ze^{\bar{\kappa}a}}{1+\bar{\kappa}a}\right)^2 \sum_{i<j} \lambda_B \frac{e^{-\bar{\kappa}R_{ij}}}{R_{ij}} - \sum_{i<j} Z^2 \frac{\lambda_B}{R_{ij}} + \beta\Phi. \tag{2.42}$$

Where the volume term was defined by

$$\frac{\beta\Phi}{V} = \sum_{i=\pm} \bar{\rho}_i\big(\ln\frac{\bar{\rho}_i}{\rho_s} - 1\big) - \frac{1}{2}\frac{(Zn)^2}{\bar{\rho}_+ + \bar{\rho}_-} + \frac{\eta}{1-\eta}\frac{2\bar{\rho}_+\bar{\rho}_-}{\bar{\rho}_+ + \bar{\rho}_-} - \frac{n}{2}\frac{Z^2\bar{\kappa}\lambda_B}{1+\bar{\kappa}a}, \tag{2.43}$$

which does not depend on the colloidal coordinates. It is called the volume term, since it is a density-dependent, extensive thermodynamic quantity that scales with the volume of the system.

Consider the colloid-colloid interaction H_{cc}, which is simply given, outside the colloids, by a sum of Coulomb repulsions $\beta H_{cc} = Z^2 \sum_{i<j} \frac{\lambda_B}{R_{ij}}$. Notice that the total thermodynamic energy of the system is

$$\beta(H_{cc} + \Omega) = \left(\frac{Ze^{\bar{\kappa}a}}{1+\bar{\kappa}a}\right)^2 \sum_{i<j} \lambda_B \frac{e^{-\bar{\kappa}R_{ij}}}{R_{ij}} + \beta\Phi. \tag{2.44}$$

From here the pair potential $U_2(r)$ is easily recognized,

$$\beta U_2(r) = \begin{cases} \infty, & r < 2a \\ \left(\frac{Ze^{\bar{\kappa}a}}{1+\bar{\kappa}a}\right)^2 \lambda_B \frac{e^{-\bar{\kappa}r}}{r}, & r > 2a. \end{cases} \tag{2.45}$$

What follows from (2.45) is that colloids in a ionic solution do not interact via a Coulomb potential, but with a Yukawa potential with a screening length $\bar{\kappa}$. The physical picture one should have in mind is that, when the colloids are suspended, anions surround the colloids and "screen" the interaction between them. Because of this extra layer of charge surrounding the colloids it will appear, from a distance, that the charge of a colloid is not Z, but $\frac{Ze^{\bar{\kappa}a}}{1+\bar{\kappa}a}$. In the next section an alternative method to calculate the charge normalization will be shown, which corresponds to this physical picture.

2.1.6 DLVO-theory: A physical approach

We will now derive DLVO-theory from a more physical perspective as in Ref. [1], in which the origin of the charge normalization becomes clear. Instead of dealing with colloids of radius a, assume that the colloids are point particles with charge Z. Starting from the PB-equation (2.24), consider an expansion around $\tilde{\phi}$, up to first order,

$$\nabla^2\phi(\mathbf{r}) = \kappa^2\Big(\sinh\tilde{\phi} + (\phi(\mathbf{r}) - \tilde{\phi})\cosh\tilde{\phi}\Big) - Z\lambda_B \sum_{i=1}^{N} \delta(|\mathbf{r} - \mathbf{R}_i|). \tag{2.46}$$

Taking $\tilde{\phi} = 0$ gives the easiest form of the linearized PB-equation,

$$\nabla^2\phi(\mathbf{r}) = \kappa^2\phi(\mathbf{r}) - Z\lambda_B \sum_{i=1}^{N} \delta(|\mathbf{r} - \mathbf{R}_i|). \tag{2.47}$$

This corresponds to linearizing the ion-densities $\rho_\pm(\mathbf{r})$ in (2.23),

$$\rho_\pm(\mathbf{r}) = \rho_s(1 \mp \phi(\mathbf{r})). \tag{2.48}$$

One can check that the solution to (2.47) is given by

$$\phi(\mathbf{r}) = \sum_{j=1}^{N} \phi_1(|\mathbf{r} - \mathbf{R}_j|; Z), \tag{2.49}$$

with $\phi_1(r; Z) = Z\lambda_B \frac{\exp(-\kappa r)}{r}$ the one-particle potential. Suppose that we now take a sphere S_i of radius a with colloid i at its center. The total charge Q_i inside this sphere, assuming that the other colloids are not inside this sphere, is given by

$$\begin{aligned} Q_i &= Z + \int_{S_i} d\mathbf{r}\Big(\rho_+(\mathbf{r}) - \rho_-(\mathbf{r})\Big) \\ &= Z - 2\rho_s \int_{S_i} d\mathbf{r}\phi(\mathbf{r}) \\ &= Z - 2\rho_s \int_{S_i} d\mathbf{r} \sum_{j=1}^{N} \phi_1(|\mathbf{r} - \mathbf{R}_j|; Z). \end{aligned} \tag{2.50}$$

By assuming that the other colloids are sufficiently far away from colloid i, such that $\sum_{j=1}^{N} \phi_1(|\mathbf{r} - \mathbf{R}_j|; Z) \approx \phi_1(|\mathbf{r} - \mathbf{R}_i|; Z)$ inside S_i, and assuming that colloid i is at the origin of the coordinate system, the total charge becomes

$$\begin{aligned} Q_i &= Z - 2\rho_s \int_{S_i} d\mathbf{r}\phi_1(|\mathbf{r} - \mathbf{R}_i|; Z) \\ &= Z - 2\rho_s \int_{S_i} d\mathbf{r} Z\lambda_B \frac{\exp(-\kappa|\mathbf{r}|)}{|\mathbf{r}|} \\ &= Z - Z8\pi\lambda_B\rho_s \int_0^a dr\ r^2 \frac{\exp(-\kappa r)}{r} \\ &= Z(1 + \kappa a)\exp(-\kappa a). \end{aligned} \tag{2.51}$$

Putting this relation back into the one-particle potential gives the usual DLVO-form,

$$\phi_1(\mathbf{r}; Z) = \frac{Q_i \exp(\kappa a)}{1 + \kappa a} \lambda_B \frac{\exp(-\kappa|\mathbf{r} - \mathbf{R}_i|)}{|\mathbf{r} - \mathbf{R}_i|}. \tag{2.52}$$

There are were also attempts in which one does not make the assumption that the other particles are far away, such as in Ref. [8]. In this case one uses the one-particle

densities (2.39) to compute the charge $\tilde{Q}_i$ inside S_i induced by the other colloids. One is interested in computing

$$\begin{aligned}\tilde{Q}_i &= \int_{S_i} d\mathbf{r} \sum_{j\neq i}^{N} \rho_1(|\mathbf{r}-\mathbf{R}_j|) \\ &= \frac{1}{(2\pi)^3} \sum_{j\neq i}^{N} \int_{S_i} d\mathbf{r} \int d\mathbf{k} \frac{Z\kappa^2}{4\pi} \frac{e^{-i\mathbf{k}\cdot\mathbf{R}_j} e^{\kappa a}}{1+\kappa a} \frac{4\pi}{k^2+\kappa^2} e^{i\mathbf{k}\cdot\mathbf{r}}, \end{aligned} \tag{2.53}$$

where we Fourier transformed the one-particle density by using the standard Fourier transform for a Yukawa potential. This integral needs to be evaluated by using contour integration, for details see Ref. [8]. After some algebra one finds

$$\tilde{Q}_i = -\frac{Ze^{\kappa a}}{1+\kappa a} \frac{1}{\kappa} (\kappa a \cosh(\kappa a) - \sinh(\kappa a)) \sum_{j\neq i}^{N} \frac{e^{-\kappa|\mathbf{R}_j|}}{|\mathbf{R}_j|}. \tag{2.54}$$

Although it is tempting to now redefine the effective charge such that it compensates for the build up of ionic charge caused by the other colloids, one should be careful with this, see Ref. [8]. By introducing a larger charge in this way one also increases the number of counter-ions and the total charge of the double layer is hereby also increased. This means that one should now repeat the above calculation for the redefined charge to correct for this. This process needs to be repeated indefinitely and it is not clear that a limiting value exists.

Finally we want to check the validity of the DLVO theory as a function of the dimensionless combination κa. Suppose a Debye length $1/\kappa = da$ is given for some dimensionless value d. This means that the size of the double layer is d times the size of the colloids. Further suppose that there are two colloids of radius a in a volume V at distance L, where the volume is equally divided over the two colloids in a spherical way, see Fig. 2.2. The packing fraction in this system is given by

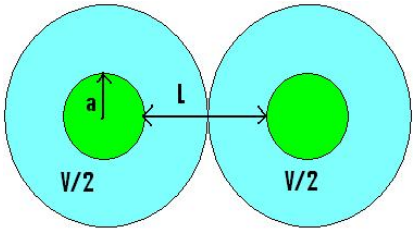

Figure 2.2: Two colloids of radius a in a equally spherically distributed volume V at a surface-to-surface distance L.

$$\begin{aligned}\eta &= \frac{4/3\pi a^3}{4/3\pi(\frac{1}{2}L+a)^3} \\ &= \Big(\frac{a}{\frac{1}{2}L+a}\Big)^3 \\ \Rightarrow L &= 2a(\eta^{-1/3}-1). \end{aligned} \tag{2.55}$$

When we agree that DLVO-theory is valid if the colloids are more than one screening length apart, i.e. the ion distribution around each colloid is mainly caused by the colloid itself, the following regimes can be discriminated:

$$\begin{aligned} L > \frac{1}{\kappa} \quad &\Rightarrow \quad 2(\eta^{-1/3}-1) > d, && \text{DLVO regime,} \\ L = \frac{1}{\kappa} \quad &\Rightarrow \quad 2(\eta^{-1/3}-1) = d, && \text{transition point,} \\ L < \frac{1}{\kappa} \quad &\Rightarrow \quad 2(\eta^{-1/3}-1) < d, && \text{non-DLVO regime.} \end{aligned}$$

Now consider the following limits:

$$\begin{aligned} d \to 0 \quad (\kappa a \to \infty): &\quad \text{DLVO theory is valid for all } 0 \leq \eta \leq 1. \\ d \to \infty \quad (\kappa a \to 0): &\quad \text{non-DLVO regime for all } 0 \leq \eta \leq 1. \end{aligned} \tag{2.56}$$

For high κa we thus expect DLVO theory to work very well even at high densities, while for low κa we expect DLVO theory to be a poor approximation for the actual grand potential of the system. The physical picture one should keep in mind is that DLVO theory works well for weakly overlapping double layers.

2.2 Crystal structures and phase transitions

In the previous section we derived the pair potential (2.45) for colloids suspended in a ionic solution. This derivation did not assume any ordering of the colloids in the solution, while it is well known that colloids can form highly ordered crystal structures as mentioned in Ref. [1, 3]. In this section we will explore some of the features this extra structure induces. First Wigner-Seitz cells and their spherical approximations are discussed, subsequently face centered cubic (fcc) and body centered cubic (bcc) crystal structures are treated and DLVO-theory is applied to them in order to find a bcc-fcc phase transition. Finally some remarks are made on dielectric constant ratios between colloid and suspension.

2.2.1 Wigner-Seitz cells

Suppose that a configuration of colloids, with coordinates $\{\mathbf{R}_i\}$, is given. To construct the Wigner-Seitz (WS) cells for this system, draw lines between each set of

coordinates $\mathbf{R}_i$ and $\mathbf{R}_j$, find the middle point of each line and draw a plain perpendicular to each line through its middle point. The Wigner-Seitz cell then consist of all the points around the colloid which can be connected to the colloid by a straight line which does not intersect with such a plain, see Figure 2.3. For a general colloid configuration the Wigner-Seitz cell around each colloid looks different, but when considering a regular crystal all the cells become equivalent to each other (ignoring finite system size effects). One appealing feature that can be deduced from this is that each cell must be charge neutral, since, if we suppose the opposite, the entire system would have a net charge, while it was assumed that the system is charge neutral. This means that the electric field flux through each cell must vanish. Furthermore the grand potential of the entire system is just N times the grand potential of an individual cell. This property is used to reduce the calculation of the grand potential of the entire system to the calculation of the grand potential of a single cell.

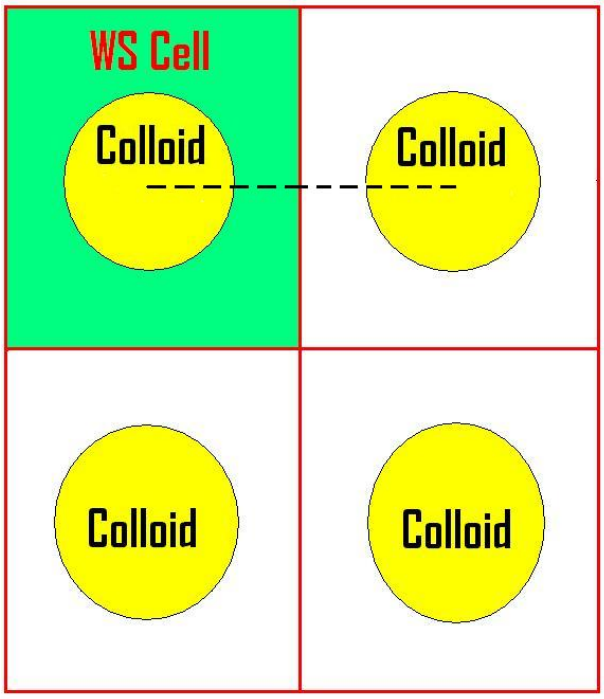

Figure 2.3: 2D-impression of colloids (yellow) in a WS cell (green). The cell's boundary (red) is given by the lines perpendicular to the lines connecting the centers of the colloids (black dotted).

Grand-potential of a Wigner-Seitz cell

Taking into account colloid-colloid, colloid-ion and ion-ion interactions, the grand-potential functional $\Omega_{\mathsf{WSC}}[\rho_+, \rho_-]$ as defined in equation (2.21) for a WS cell is given by

$$\begin{aligned}\beta\Omega_{\mathsf{WSC}} = \frac{1}{2}\int_{\mathsf{cell}} d\mathbf{r}\rho_+(\mathbf{r})(\log\left[\frac{\rho_+(\mathbf{r})}{\rho_s}\right] - 1) + \rho_-(\mathbf{r})(\log\left[\frac{\rho_-(\mathbf{r})}{\rho_s}\right] - 1) \\ + [\rho_+(\mathbf{r}) - \rho_-(\mathbf{r}) + q(\mathbf{r})]\phi(\mathbf{r}),\end{aligned} \tag{2.57}$$

with $q(\mathbf{r})$ the colloidal charge distribution and $\phi(\mathbf{r})$ the dimensionless potential given by (2.22). In linear PB-theory terms $O(\phi(\mathbf{r})^4)$ are ignored and by making the substitution $\rho_\pm(\mathbf{r}) = \rho_s(1 \mp \phi(\mathbf{r}))$ the grand-potential becomes

$$\beta\Omega_{\mathsf{WSC}} = \frac{1}{2}\int_{\mathsf{cell}} d\mathbf{r}q(\mathbf{r})\phi(\mathbf{r}), \tag{2.58}$$

where we have ignored a constant volume term, since the grand-potential is defined up to a constant.

Spherical Wigner-Seitz cells

In order to simplify the calculation of the electrostatic potential $\phi(\mathbf{r})$ by using the PB-equation (2.24) or the linear PB-equation (2.47)* an approximation was developed which transforms the WS cells to spherical WS cells [9]. In this approximation the packing fraction $\eta = V_{\mathsf{colloid}}/V_{\mathsf{cell}}$ is kept constant, such that the radius R of the spherical cell equals $R = a\eta^{-1/3}$. Also, the cell remains charge neutral. In this approximation the (linear) PB-equation becomes a one-dimensional differential equation,

$$\begin{aligned}\frac{\partial^2\phi}{\partial r^2}(r) + \frac{2}{r}\frac{\partial\phi}{\partial r}(r) &= \kappa^2\sinh(\phi(r)) \quad \text{- non-linear case} \\ \frac{\partial^2\phi}{\partial r^2}(r) + \frac{2}{r}\frac{\partial\phi}{\partial r}(r) &= \kappa^2\phi(r) \quad \text{- linear case} \\ \frac{\partial\phi}{\partial r}(a) = -\frac{Z\lambda_B}{a^2}; &\quad \frac{\partial\phi}{\partial r}(R) = 0.\end{aligned} \tag{2.59}$$

A sample solution for the non-linear case in given in Fig. 2.4. Spherical WS cells play an important role in the numerical model that is the subject of this thesis, which is discussed in chapter 3.

2.2.2 fcc and bcc crystal structures

If a crystal is given, a (primitive) unit cell for this crystal is a small box containing a fixed number of colloids (or atoms) in a specific configuration, such that when such

*The spherical approximation to Wigner-Seitz cells is usually used only in non-linear Poisson-Boltzmann theory. However, since in this thesis the numerical calculations are done in the linear theory, we will consider the spherical approximation also in the linear case.

cells are stacked the entire crystal is reproduced. In the case that the unit cell has the shape of a cube, we call the crystal a cubic crystal. The two most important cubic crystals are face-centered cubic (fcc) crystals and body-centered cubic (bcc) crystals, their unit cells are depicted in Fig. 2.5.

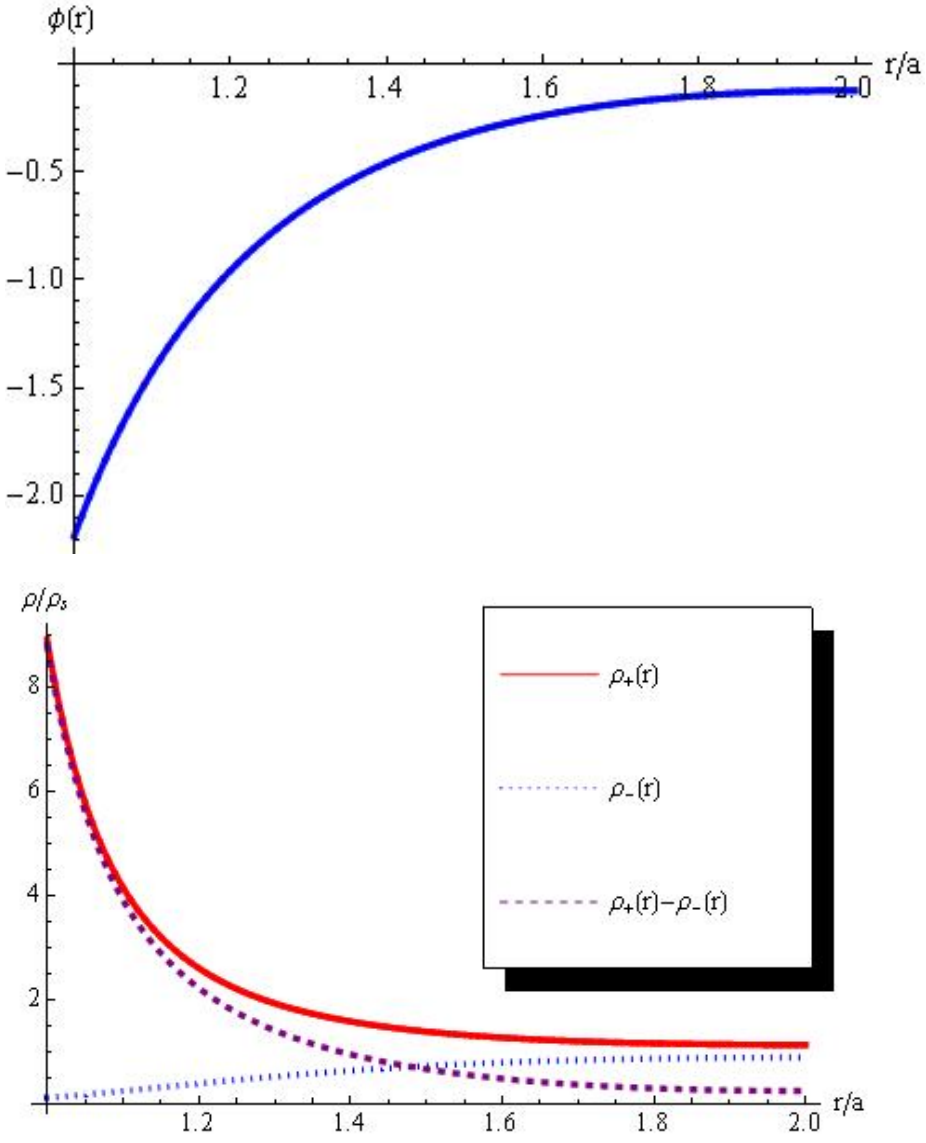

Figure 2.4: A sample solution for the non-linear PB-equation, Eq. (2.59), with $\kappa a = 3$, $a/\lambda_B = 100$ and $Z = 1000$. The top figure shows the potential $\phi(r)$ and the bottom figure shows the corresponding ion-densities $\rho_{\pm}(r)$ and total density $\rho(r) = \rho_+(r) - \rho_-(r)$.

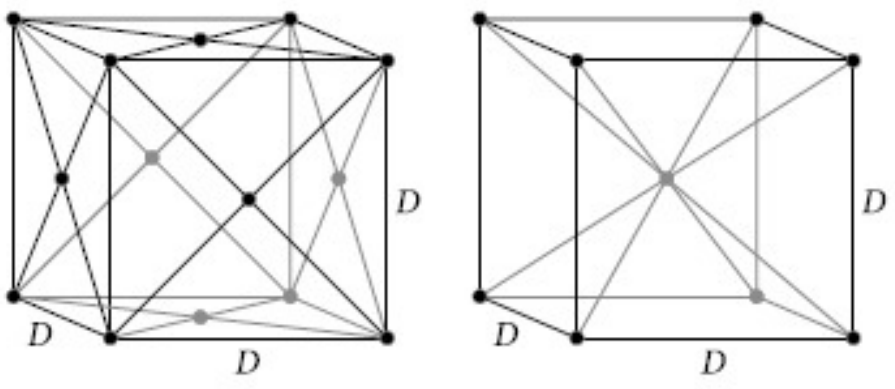

Figure 2.5: Cubic unit cells of fcc (left) and bcc (right) crystal structures with cubic lattice spacing D. Source: Ref. [3]

The fcc crystal

The fcc crystal is also called cubic close-packed, since it can be build up from hexagonal layers of closed packed planes. The number of particles in the unit cell is equal to 14, from which six are shared with one other unit cell and eight are shared with seven other unit cells. This gives an effective four particles in a fcc unit cell. The maximal packing fraction in this structure is $\eta_{\text{fcc,max}} = \dfrac{\pi\sqrt{2}}{6} \approx 0.74$, which can be easily calculated with elementary geometry. A convenient basis, for a cubic unit cell with edge length D, in this structure is

$$\begin{cases} \mathbf{e}_1 = \frac{D}{2}(1,1,0) \\ \mathbf{e}_2 = \frac{D}{2}(1,0,1) \\ \mathbf{e}_3 = \frac{D}{2}(0,1,1). \end{cases} \tag{2.60}$$

The Wigner-Seitz cell for a fcc structure is given by a rhombic dodecahedron (Fig. 2.6). Examples of elements that crystallize into the fcc structure are aluminium, calcium, nickel, copper, silver, gold, lead, neon, argon, krypton and xenon [10].

The bcc crystal

The bcc crystal structure is less close-packed than the fcc crystal structure. The number of particles in the unit cell equals nine, from which eight are shared with seven other unit cells. This gives effectively two particles in the unit cell. The maximal packing fraction in this structure is $\eta_{\text{bcc,max}} = \dfrac{\pi\sqrt{3}}{8} \approx 0.68$. A basis, for a cubic unit cell with edge length D, that will turn out to be convenient is given by

$$\begin{cases} \mathbf{e}_1 = \frac{D}{2}(-1,1,1) \\ \mathbf{e}_2 = \frac{D}{2}(1,-1,1) \\ \mathbf{e}_3 = \frac{D}{2}(1,1,-1), \end{cases} \tag{2.61}$$

The Wigner-Seitz cell for a bcc structure is given by a truncated octahedron (Fig. 2.7). Some elements that crystallize into the bcc crystal structure are lithium, sodium, potassium, chromium, barium and tungsten [10].

2.2.3 Grand-potential of a WS cell in the fcc and bcc crystal structures

We want to compute the grand-potential of a system of colloids in either a bcc or fcc crystal. To simplify this calculation we will assume that the colloids are point-particles with a charge Z, such that the charge distribution for colloid i is given by $q_i(\mathbf{r}) = Z\delta(|\mathbf{r} - \mathbf{R}_i|)$. In the case of point-particles DLVO theory and the WS cell approach give the same expression for the grand-potential. Using the pair potential Eq. (2.45) the grand-potential of the system is given by

$$\Omega_{\text{DLVO}} = Z^2\lambda_B \sum_i \sum_{j>i} \frac{e^{-\kappa|\mathbf{R}_i - \mathbf{R}_j|}}{|\mathbf{R}_i - \mathbf{R}_j|}. \tag{2.62}$$

Notice that by evaluating equation (2.58) for the point-charge distribution, combined with the solution $\phi(\mathbf{r})$ in linear PB-theory given by (2.49), gives the following grand-potential for a Wigner-Seitz cell around a colloid with coordinate $\mathbf{R}_0$,

$$\beta\Omega_{\text{WSC}} = \frac{Z}{2}\phi(\mathbf{R}_0) = \frac{Z^2\lambda_B}{2} \sum_{i\neq 0} \frac{e^{-\kappa|\mathbf{R}_i - \mathbf{R}_0|}}{|\mathbf{R}_i - \mathbf{R}_0|}. \tag{2.63}$$

From this equation it follows that the grand-potential of the total crystal is indeed N times the grand-potential of a single cell. Following Ref. [3] we will evaluate the Yukawa summation in Eq. (2.63).

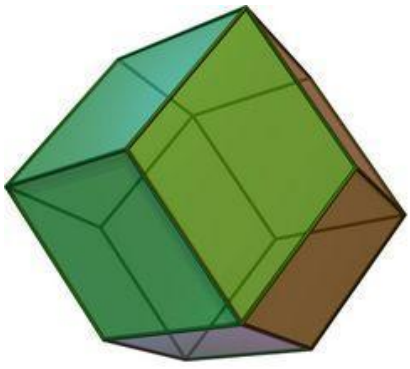

Figure 2.6: Wigner-Seitz cell for the fcc crystal structure, the rhombic dodecahedron. Source: wikipedia

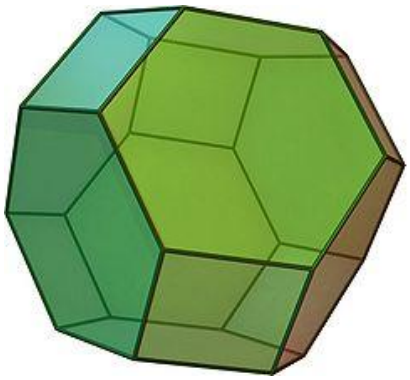

Figure 2.7: Wigner-Seitz cell for the bcc crystal structure, the truncated octahedron. Source: wikipedia

This can be done most easily by introducing the following: let N_j be the number of colloids at a distance d_j from the colloid at position $\mathbf{R}_0$. With these definitions the sum (2.63) can be rewritten as

$$\beta\Omega_{\mathsf{WSC}} = \frac{Z^2\lambda_B}{2}\sum_{j\neq 0} N_j \frac{\exp(-\kappa d_j)}{d_j}. \tag{2.64}$$

The sum still depends on the crystal structure. We will compute it numerically for the fcc and bcc crystal structure by making use of the previously defined bases.

Grand-potential of a fcc crystal

Using the basis (2.60), an arbitrary colloid's position can be denoted $\mathbf{r} = n_1\mathbf{e}_1 + n_2\mathbf{e}_2 + n_3\mathbf{e}_3$, with n_1, n_2, n_3 integers. The norm of this vector is given by

$$\|\mathbf{r}\| = \frac{D}{\sqrt{2}}\sqrt{(n_1^2+n_2^2+n_3^2)+(n_1n_2+n_1n_3+n_2n_3)}. \tag{2.65}$$

By considering all values of n_1, n_2, n_3 all distances d_j are generated and by counting the number of occurrences of that particular distance the sum (2.64) can be evaluated. For practical purposes, however, it is more convenient to take a large cut-off value n_{max} for n_1, n_2, n_3 and compute the distances and number of occurrences numerically. For later use define $d_{j,fcc} = \frac{D}{\sqrt{2}}\sqrt{j}$, where j is an positive integer number. Notice that this agrees with (2.65).

Grand-potential of a bcc crystal

Similarly as in the fcc case, an arbitrary colloid position can be denoted $\mathbf{r} = n_1\mathbf{e}_1 + n_2\mathbf{e}_2 + n_3\mathbf{e}_3$, but now with respect to the basis (2.61). The norm of this vector equals

$$\|\mathbf{r}\| = \frac{D}{2}\sqrt{3(n_1^2+n_2^2+n_3^2)-2(n_1n_2+n_1n_3+n_2n_3)}. \tag{2.66}$$

Again, we can now compute all distances and number of occurrences by using a numerical method. Define $d_{j,bcc} = \frac{D}{2}\sqrt{j}$, with j a positive integer.

Introduction of dimensionless parameter

Before computing the grand-potential of the fcc and bcc structures, it is convenient to introduce a dimensionless parameter $\lambda = \kappa a_0$, where a_0 is the natural length scale of the system, i.e. $a_0 = (N/V)^{-1/3}$, where N is the number of colloids in the volume V. To compute a_0 for the structures we are interested in we take the volume to be equal to that of the unit cell, $V = D^3$. In a fcc unit cell there are effectively four particles and in a bcc unit cell there are two. From this it follows that $a_{0,fcc} = D/2^{2/3}$ and $a_{0,bcc} = D/2^{1/3}$. We have thus found the following expressions for the grand-potential of the crystal structures

$$\beta\Omega_{\mathsf{WSC,fcc}} = \frac{Z^2\kappa}{2}\lambda_B \sum_{j=1}^{\infty} N_{j,\mathsf{fcc}} \frac{\exp(-2^{1/6}\lambda\sqrt{j})}{2^{1/6}\lambda\sqrt{j}} \tag{2.67}$$

$$\beta\Omega_{\mathsf{WSC,bcc}} = \frac{Z^2\kappa}{2}\lambda_B \sum_{j=1}^{\infty} N_{j,\mathsf{bcc}} \frac{\exp(-2^{-2/3}\lambda\sqrt{j})}{2^{-2/3}\lambda\sqrt{j}}. \tag{2.68}$$

For later use we will also consider the dimensionless parameter for finite size colloids with radius a. In this case one has to make use of the definition of the packing fraction $\eta = 4N\pi a^3/3V$. Combining this with the definition of λ by elimination of N gives the relation

$$\lambda = (\frac{4\pi}{3\eta})^{1/3}\kappa a. \tag{2.69}$$

From this expression it is clear that at maximal packing fraction η_{max} increasing κa leads to larger minimal value of λ. In order to compensate for this, we will often make use of the variable $\lambda - \lambda_0$, with $\lambda_0 = (4\pi/3\eta_{\mathsf{max}})^{1/3}\kappa a$. Notice that this variable is, up to a scaling factor, a measure of the colloid-colloid distance in units of the Debye length $1/\kappa$. In table 2.1 $\lambda_0/\kappa a$ is listed for some crystal structures.

Table 2.1: $\lambda_0/\kappa a$ for different crystal structures.

	Cube	fcc	bcc
$\lambda_0/\kappa a$	2.00	1.80	1.83

2.2.4 fcc/bcc phase transition

By determining the zero point (and thus the critical value λ_c) of $\beta\Delta\Omega = \beta(\Omega_{\mathsf{WSC,bcc}} - \Omega_{\mathsf{WSC,fcc}})$ an energy dominated strong coupling phase transition is found. This means that only the energy of the colloids is taken into account for this phase transition and not their entropy. The physical picture corresponding to this is a system of colloids which are pinned-down to their lattice positions by, for instance, a strong repulsion

between them due to high values of colloid charge Z. We call this a $T = 0$ phase transition, although there is still a non-zero temperature for the salt ions, or else double layers would not be formed.

It is clear from (2.67) and (2.68) that λ_c does not depend on the system parameters. In Fig. 2.8, $\beta\Delta\Omega$ is plotted as a function of λ. The critical value is $\lambda_c \approx 1.74$ and the system is in the bcc phase for $\lambda < \lambda_c$ and in the fcc phase for $\lambda > \lambda_c$, which agrees with literature [11]. An important remark for the data in Fig. 2.8 is that the order of magnitude of $\beta\Delta\Omega$ is very small compared to the prefactor. The order of the grand-potential difference is 10^{-4}, when the prefactor is of order 1. Notice, however, that this does not imply that the actual difference in grand-potential energy between bcc and fcc is small, because by adding more charge to the colloids the energy difference becomes larger.

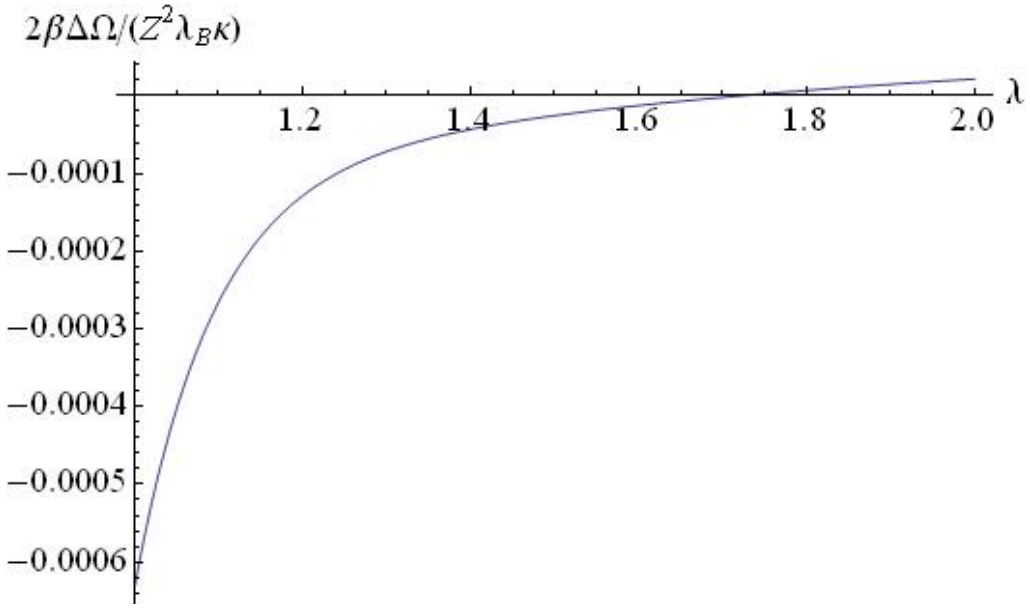

Figure 2.8: The difference $\beta\Delta\Omega$ between fcc and bcc cell in units of the prefactor $Z^2\lambda_B\kappa/2$ as a function of λ. The critical value λ_c for the bcc/fcc phase transition can be determined to be equal to $\lambda_c \approx 1.74$. For $\lambda < \lambda_c$ the system is in the bcc phase and for $\lambda > \lambda_c$ the system is in the fcc phase.

Chapter 3

Non-Spherical Wigner-Seitz cells

As mentioned in the previous chapter, it is usual in non-linear PB-theory to approximate general WS cells by spherical WS cells. The drawback of this approximation is that it does not allow non-uniform potential or charge distribution over the colloid surface. In this chapter we will describe a model that allows to solve the PB-equation for general WS cells. This will, however, be done in the linear approximation for the following reason. Since we do not know how big the effect of non-uniform surface potentials or charge distributions is, its properties are best explored first with the linear PB-equation, for which the numerical implementation is relatively easy. Also, exact expressions exist for the grand potential of a system of point particles in various crystal structures in linear approximation, see chapter 2, which can be compared with the numerical results of the model to check consistency. If it turns out that the effect of non-uniformity is indeed significant, the linear model can be used as a stepping stone to implement the non-linear model. In this thesis we will only consider fixed surface charge distributions.

3.1 The linear PB-equation in spherical harmonics

Consider the linear PB-equation as defined in (2.47), but now for finite size colloids with radius a,

$$\nabla^2\phi(\mathbf{r}) = \kappa^2\phi(\mathbf{r}) - \frac{Z\lambda_B}{a^2}\sum_{i=1}^{N}\delta(|\mathbf{r}-\mathbf{R}_i|-a). \tag{3.1}$$

Change the Cartesian coordinates to spherical coordinates, $(x,y,z)\to(r,\theta,\varphi)$, and expand the potential in spherical harmonics (see Appendix A),

$$\phi(r,\theta,\varphi) = \sum_{l=0}^{\infty}\sum_{m=-l}^{l} f_m^l(r)Y_m^l(\theta,\varphi). \tag{3.2}$$

Plugging this back into (3.1) and using that the spherical harmonics are eigenfunctions of ∇^2, i.e. $r^2\nabla^2 Y_m^l(\theta,\varphi) = -l(l+1)Y_m^l(\theta,\varphi)$, gives (ignoring boundary conditions for now)

$$\begin{aligned}\nabla^2\phi(\mathbf{r}) &= \sum_{l=0}^{\infty}\sum_{m=-l}^{l}\Big\{[\nabla^2 f_m^l(r)]Y_m^l(\theta,\varphi) + f_m^l(r)[\nabla^2 Y_m^l(\theta,\varphi)]\Big\} \\ &= \sum_{l=0}^{\infty}\sum_{m=-l}^{l}\Big\{\nabla^2 f_m^l(r) - \frac{l(l+1)}{r^2}f_m^l(r)\Big\}Y_m^l(\theta,\varphi) \\ &= \kappa^2\sum_{l=0}^{\infty}\sum_{m=-l}^{l} f_m^l(r)Y_m^l(\theta,\varphi). \end{aligned} \tag{3.3}$$

Using the explicit form of the radial part of ∇^2 gives the following set of equations for the solution of the linear PB-equation,

$$\left\{\frac{\partial^2 f_m^l(r)}{\partial r^2} + \frac{2}{r}\frac{\partial f_m^l(r)}{\partial r} - \frac{l(l+1)}{r^2}f_m^l(r) = \kappa^2 f_m^l(r)\right\}_{m=-l,\ldots,l}^{l=0,\ldots,\infty}. \tag{3.4}$$

In order to find the correct boundary conditions for this system of equations, first consider the differential equation for the monopole,

$$\frac{\partial^2 f_0^0(r)}{\partial r^2} + \frac{2}{r}\frac{\partial f_0^0(r)}{\partial r} = \kappa^2 f_0^0(r). \tag{3.5}$$

Notice that this is exactly the same equation as (2.59), which described a spherical approximation for the WS cell. The boundary condition at the colloid's surface should then also be given by $\frac{\partial f_0^0}{\partial r}(a) = -\frac{Z\lambda_B}{a^2}$, since the charge of the colloid equals Ze. To find the correct boundary conditions at the colloid's surface for $l \neq 0$, consider the differential equation for the interior of the colloids ($r < a$), namely Laplace equation $\nabla^2\phi(\mathbf{r}) = 0$, which leads to the following system of equations

$$\left\{\frac{\partial^2 f_m^l(r)}{\partial r^2} + \frac{2}{r}\frac{\partial f_m^l(r)}{\partial r} - \frac{l(l+1)}{r^2}f_m^l(r) = 0\right\}_{m=-l,\ldots,l}^{l=1,\ldots,\infty}. \tag{3.6}$$

The non-diverging solution to this system of equations is given by $f_m^l(r) = k_m^l r^l$, with k_m^l an integration constant. Making use of the fact that the derivative of $f_m^l(r)$ should be continuous at the colloid's surface gives

$$\frac{\partial f_m^l}{\partial r}(a) = k_m^l l a^{l-1} = \frac{l f_m^l(a)}{a}. \tag{3.7}$$

Now the boundary conditions at the colloid's surface are set. What remains is to give another set of boundary conditions in order to completely fix the boundary value problem (3.4). We now introduce constants $\{c_m^l\}_{m=-l,\ldots,l}^{l=0,\ldots,\infty}$ and a radius $R > a$, with $\frac{\partial f_m^l}{\partial r}(R) = c_m^l$. The boundary value problem is now completely specified. In the next section this form of the PB-equation will be applied to non-spherical WS cells.

3.1.1 Dielectric ratios

Next to the boundary conditions defined above for the PB-equations, it is also possible to incorporate a difference in dielectric constant between the colloids and the solvent. Although the difference is not that big for colloidal crystals, it becomes significant and is important when considering photonic crystals [12]. Define the quantity

$$\epsilon_r = \frac{\epsilon_{colloid}}{\epsilon_{solvent}}. \tag{3.8}$$

Because of the difference in dielectric constant, at the colloid surface the boundary condition charges to

$$\frac{\partial f_m^l}{\partial r}(a) = \frac{l f_m^l(a)}{a}\epsilon_r. \tag{3.9}$$

Note that the monopole boundary condition ($l = 0$) does not change. This is because the dielectric ratio can always be scaled away by a redefinition of the Bjerrum length λ_B.

3.2 Incorporating non-spherical WS cells

Solving the linear PB-equation for a non-spherical WS cell C can now be done in the following way. Take the radius R defined previously large enough such that a sphere S with this radius includes the cell C. Solve the system of equations (3.4) on the sphere S. One now has obtained a solution depending on the constants $\{c_m^l\}$, which we denote as $\phi(\mathbf{r};\{c_m^l\})$. Define the corresponding electric field $\mathbf{E}(\mathbf{r};\{c_m^l\}) = -\nabla\phi(\mathbf{r};\{c_m^l\})$ and minimize the flux through the WS cell $\int_C \mathbf{E}(\mathbf{r};\{c_m^l\})\cdot \mathrm{d}^2\mathbf{r}$, w.r.t. the constants $\{c_m^l\}$, see Fig. 3.1.

In the ideal case described above, such a calculation leads to an exact solution for the linear PB-equation in the geometry C, by completeness of the orthogonal basis of spherical harmonics. In numerical calculations, however, a cut-off value L for the number of modes is used, i.e. the expansion of the potential in spherical harmonics becomes

$$\phi(r,\theta,\varphi) = \sum_{l=0}^{L}\sum_{m=-l}^{l} f_m^l(r)Y_m^l(\theta,\varphi). \tag{3.10}$$

This means that one needs to define a precision δ_{flux} which defines a maximal value for the flux and another precision δ_{change} which defines the minimal change in flux per iteration routine. The recipe to solve the PB-equation for non-spherical WS cells can be summarized by the following procedure:

1. Define starting values for the constants $\{c_m^l\}$.

2. Solve the system of equations (3.4) on the sphere S.

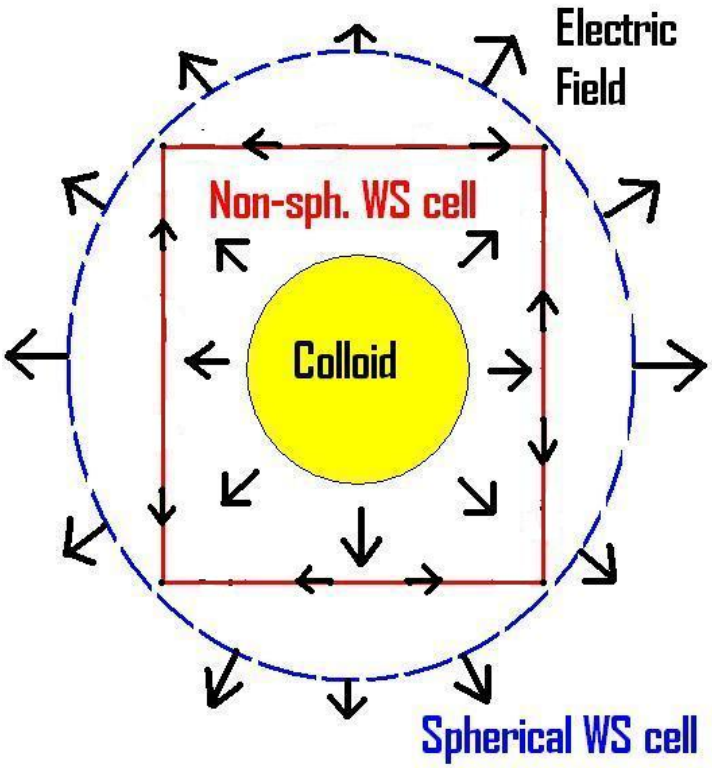

Figure 3.1: Graphical representation of the routine used to solve the PB-equation in a non-spherical geometry. The flux for each mode (l, m) is varied on the spherical WS cell surrounding the non-spherical cell in such a way that the flux through the non-spherical WS cell vanishes.

3. Compute the flux through the WS cell $\int_C \mathbf{E}(\mathbf{r}; \{c_m^l\}) \cdot \mathrm{d}\mathbf{r}$ and by using a minimization routine (see appendix B) obtain new values $\{c_m'^l\}$.

4. If $|\int_C \mathbf{E}(\mathbf{r}; \{c_m^l\}) \cdot \mathrm{d}\mathbf{r}| > \delta_{\text{flux}}$ and $\sum_{l=0}^{L} \sum_{m=-l}^{l} |c_m'^l - c_m^l| > \delta_{\text{change}}$ return to step 2, else the (approximate) solution is obtained.*

The solution that is obtained in this way still depends on numerical parameters, such as the number of modes L used, the number sample points on the WS cells C and the specific grid used for computing the potential on the sphere S. The physical solution should not depend on such parameters and to make sure the solution obtained does not depend on them, one must check that refining this parameters does not (significantly) change the solution. If one obtains a stable solution in this manner, it becomes possible to look at the physical implications of the results of such a numerical calculation.

*Other criteria are also possible. The ones mentioned here are used in the numerical implementation for this thesis.

3.3 Low packing fraction limit

In order to ensure that the results one obtains from a new numerical model are consistent with existing literature it is important to formulate a number of consistency checks. For this particular model there will be some checks originating from chapter 2.

The first two checks correspond to checking that minimal functionality is obtained. We expect peaks in the zeta-potential of the colloid at the places which are closest to the other colloids, because it will cost more energy for a charge to be at such a place. The other check is that the electric field decreases, in the WS cell, the further one is removed from the colloid.

In chapter 2 we derived that DLVO-theory is valid when the colloids are far apart from each other. This means that our model must have a "DLVO-limit", i.e. when the packing fraction $\eta \to 0$ we must have for the energy E_{WSC} of our model that it goes to the energy E_{DLVO} for the same system in DLVO-theory, $E_{\text{WSC}} \to E_{\text{DLVO}}$, as $\eta \to 0$. In correspondence with this, the critical value for the fcc/bcc phase transition must in the low κa and the low packing fraction limit also correspond with the one obtained from DLVO-theory, $\lambda_c = 1.74$ (see section 2.2.4). Furthermore we expect that in the low packing fraction limit the spherical approximation becomes a valid approximation for the fcc as well the bcc crystal structures. Notice however that when approximating the general WS cells in this way, one loses the information that is relevant for predicting energetic phase transitions. The reason why the spherical approximation is still valid is because, as was shown in section 2.2.4, the energy differences between the fcc and bcc crystal structure is very small, much smaller than the typical precision one wants to use for such an approximation. These low packing fraction limit expectations are a guide for determining whether the results obtained from numerical computation make sense.

Chapter 4

Numerical Results and Discussion

In this chapter the results obtained from numerical calculations based on the method presented in the previous chapter are discussed. We will refer to this method as the WS cell model. First it is shown that the model gives the expected qualitative results. Subsequently the implications of the non-spherical nature of the WS cell is explored. This includes the variation of the potential over the colloid surface, comparison with spherical WS cells and DLVO theory, and finally the effect of different dielectric ratios on the grand potential of the system.

4.1 Qualitative numerical results

In order to test whether the method presented in chapter 3 produces trustworthy results, it is a good check if there is qualitative agreement with the physical expectations as described in section 3.3. In Fig. 4.1 the surface potential is plotted for the fcc and bcc crystal structure at a high and low density and small and big screening length. Here we used that the physical potential $\psi(r, \theta, \varphi)$ is related to the dimensionless potential $\phi(r, \theta, \varphi)$ (Eq. (2.22)) by $\phi(r, \theta, \varphi) = e\psi(r, \theta, \varphi)/k_B T$, which allows us express the surface potential $\psi(a, \theta, \varphi)$ in mV. The first thing to notice is that the potential is indeed maximal at the places closes to other colloids, i.e. the plots display the correct potential distribution corresponding with the crystal structures, see also Fig. 2.5. Secondly we see that high density leads to a stronger potential variation over the colloid's surface than a low density. Especially when the particles are small at low densities we expect a more uniform potential distribution over the colloid's surface, which is also seen in the numerical results. Here it is also important to note that the potential scale of the colloids at low densities for fcc and bcc converges to the same values, which implies that the specific WS cell configuration becomes irrelevant for larger distances, as expected.

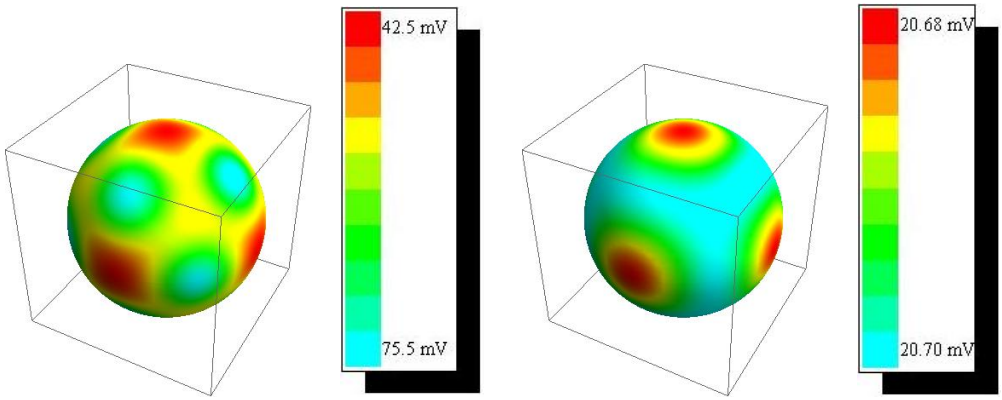

(a) Colloid in fcc structure with $\eta = 0.74$ and $\kappa a = 5$

(b) Colloid in fcc structure with $\eta = 0.1$ and $\kappa a = 0.5$

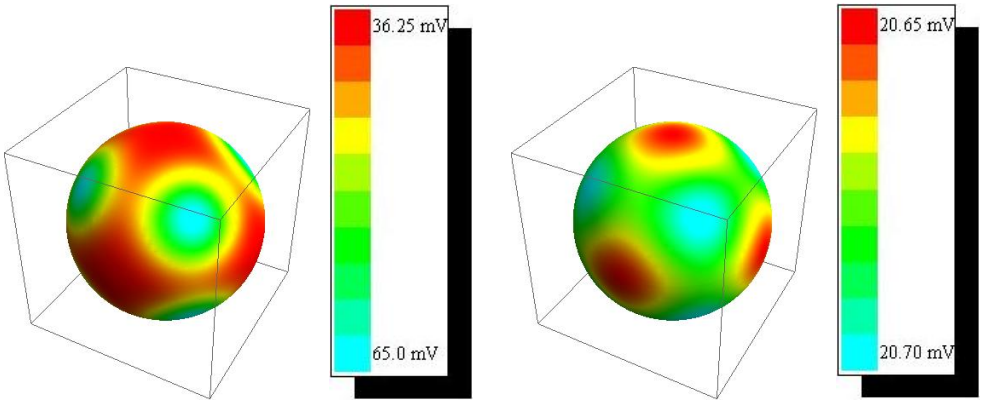

(c) Colloid in bcc structure with $\eta = 0.68$ and $\kappa a = 5$

(d) Colloid in bcc structure with $\eta = 0.1$ and $\kappa a = 0.5$

Figure 4.1: 3d images of the surface potential distribution $\psi(a, \theta, \varphi)$ of colloids of charge $Z\lambda_b/\kappa^2 a = 1$ in an fcc and a bcc lattice at various κa and packing η. The physical potential $\psi(r, \theta, \varphi)$ is related to the dimensionless potential $\phi(r, \theta, \varphi)$ defined in Eq. (2.22) by $\phi(r, \theta, \varphi) = e\psi(r, \theta, \varphi)/k_B T$.

The second check corresponds to verifying that the electric field falls off if the distance to the colloid becomes larger. This can be seen most easily in an equipotential plot such as Fig. 4.2. This figure displays a (0 0 1) slice of the fcc crystal and a (1 0 1) slice of the bcc crystal. We see indeed that the field lines lie close to each other around the colloids and get farther apart away from the colloids, indicating a decreasing electric field.

From these two qualitative results we have verified that the routine proposed in chapter 3 indeed produces meaningful information. When considering the quantitative results in the next section it is important to keep in mind the low density

requirements as explained in section 3.3. The dimensionless parameter λ we will use to present our results was defined in section 2.2.4.

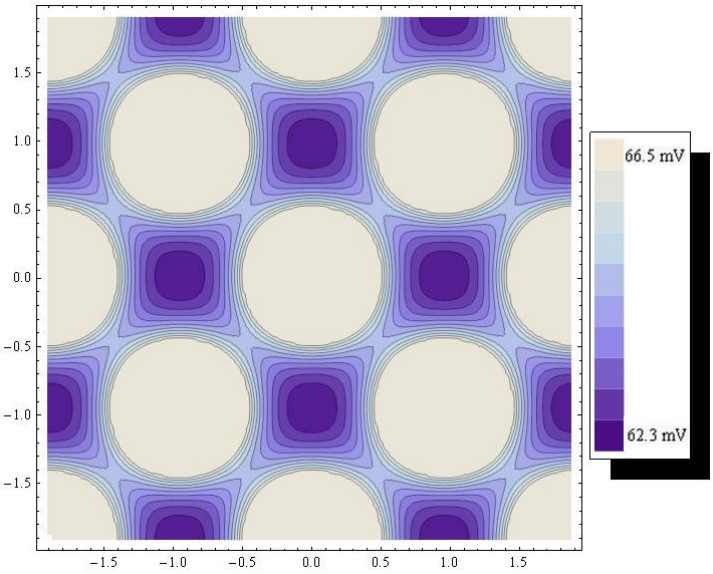

(a) Equipotential in the (0 0 1) plane for colloids in a fcc crystal.

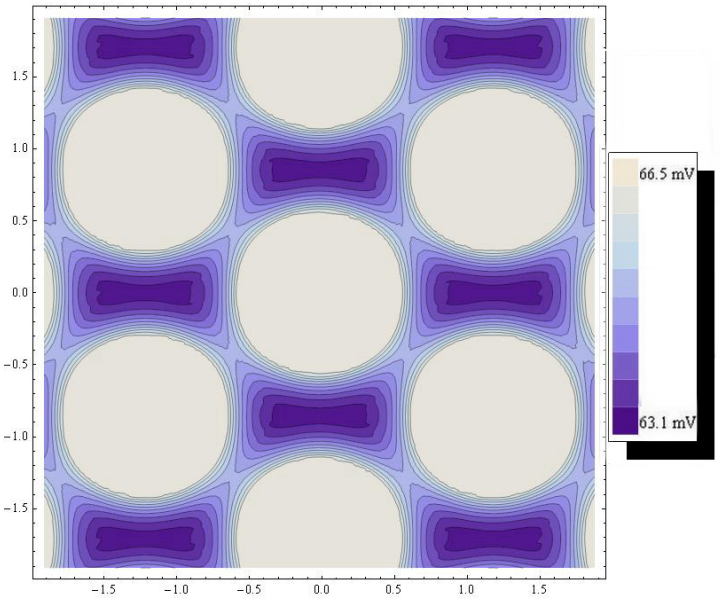

(b) Equipotential in the (1 0 1) plane for colloids in a bcc crystal.

Figure 4.2: Equipotential for colloids of charge $Z\lambda_b/\kappa^2 a = 1$ in (a) an fcc and (b) a bcc structure with in both cases $\kappa a = 0.5$ and $\eta = 0.3$. Along the vertical and horizontal axis the position is indicated in units of the colloid radius.

4.2 Potential variation and spherical approximation

In order to measure the magnitude of the non-uniform potential distribution on the colloid's surface we subtract the minimal potential $\phi_{\text{min}} = \text{Min}\{\phi(a,\theta,\varphi)|0 \leq \theta \leq 2\pi, 0 \leq \varphi \leq \pi\}$ from the maximal potential $\phi_{\text{max}} = \text{Max}\{\phi(a,\theta,\varphi)|0 \leq \theta \leq 2\pi, 0 \leq \varphi \leq \pi\}$ on the surface, see Fig. 4.3. This figure shows that for increasing κa the potential variation becomes bigger. This is because when κa becomes larger the potential distribution over a colloid's surface induced by another colloid becomes less uniform, especially when the radius of the colloids is several times the Debye length ($\kappa a > 1$).

Although this information is useful on its own, we will also express the variation in potential in percentage of the average potential of the colloid $\phi_{\text{average}} = \text{Mean}\{\phi(a,\theta,\varphi)|0 \leq \theta \leq 2\pi, 0 \leq \varphi \leq \pi\}$, see Fig. 4.4. In this way the potential variation becomes comparable with the spherical approximation (Eq. (2.59)). This means that when the variation in potential is low, the potential non-uniformity is small compared to the average potential of the colloid which we expect, at least at large distances, to be the same as in the spherical approximation. In Fig. 4.4 we see that for $\kappa a \leq 1$ the variation in potential in less than five percent at maximal packing for fcc and bcc crystals. In this case the non-uniformity in the potential distribution can be neglected and we expect the spherical approximation to be accurate in these cases. For $\kappa a > 1$ we observe that the variation cannot be neglected at high densities, so we expect in these cases that the spherical approximation differs from the WS cell model. For all the κa we see that in the low packing limit $\lambda - \lambda_0 \to \infty$ the variation goes to zero as expected. Finally we note that the variation at maximal packing fraction in a bcc cell is somewhat larger than that of an fcc cell, since the fcc cell has a more spherical nearest neighbor distribution.

In Fig. 4.5 the grand potential of a WS cell, as defined in Eq. (2.58), is plotted for the WS cell model and the spherical approximation, see Eq. (2.59). From this figure it follows that for $\kappa a \leq 1$ there is no difference between the spherical model and the WS cell model, for the fcc as well the bcc crystal. This was expected, because of the low variation in surface potential for this κa regime as mentioned before. For $\kappa a > 1$ we see that there is a noticeable difference between the two models at densities $\lambda - \lambda_0 < 1$. In this regime the potential variation becomes significant and can be seen as the main cause for this difference.

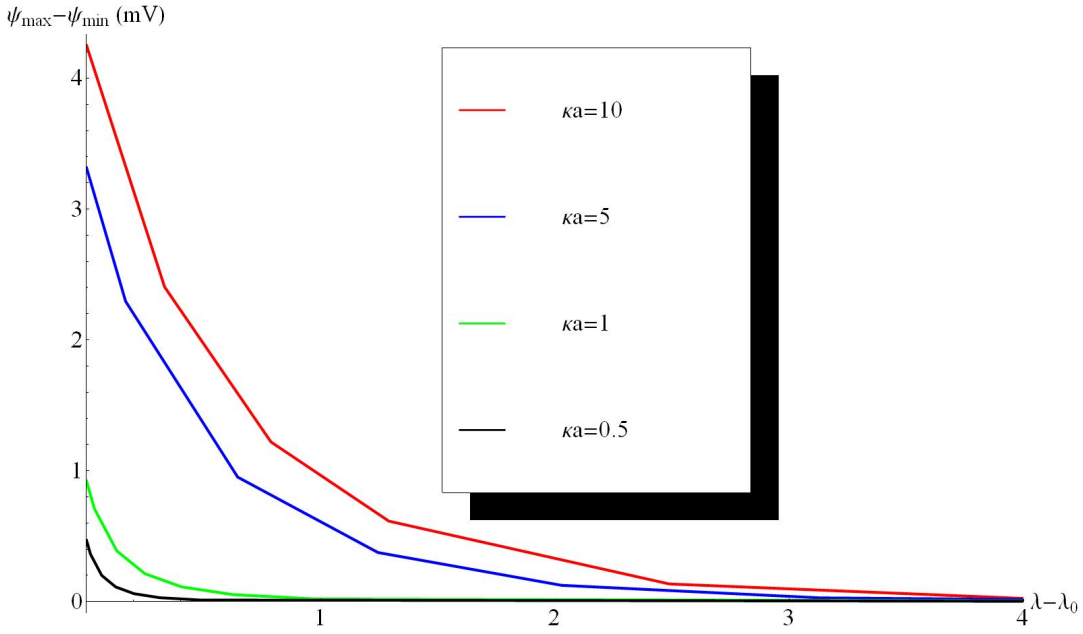

(a) Variation in potential for a colloid in an fcc lattice.

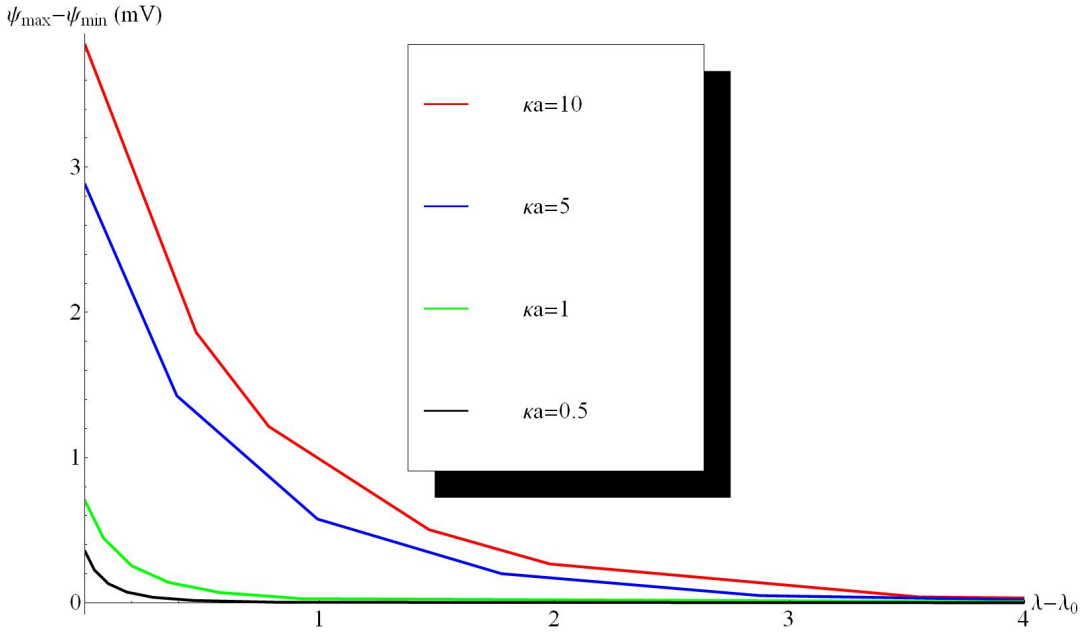

(b) Variation in potential for a colloid in a bcc lattice.

Figure 4.3: Variation in the physical surface potential $\psi_{\max} - \psi_{\min}$, which is related to the variation dimensionless surface potential defined in Eq. (2.22) by $\phi_{\max} = e\psi_{\max}/k_BT$ and $\phi_{\min} = e\psi_{\min}/k_BT$. The colloids have charge $Z\lambda_b/\kappa^2 a = 0.1$ and are in (a) an fcc and (b) a bcc crystal at various κa and are plotted as a function of $\lambda - \lambda_0$ as defined in Eq. (2.69) and below, i.e. such that $\lambda - \lambda_0 = 0$ corresponds to close packing.

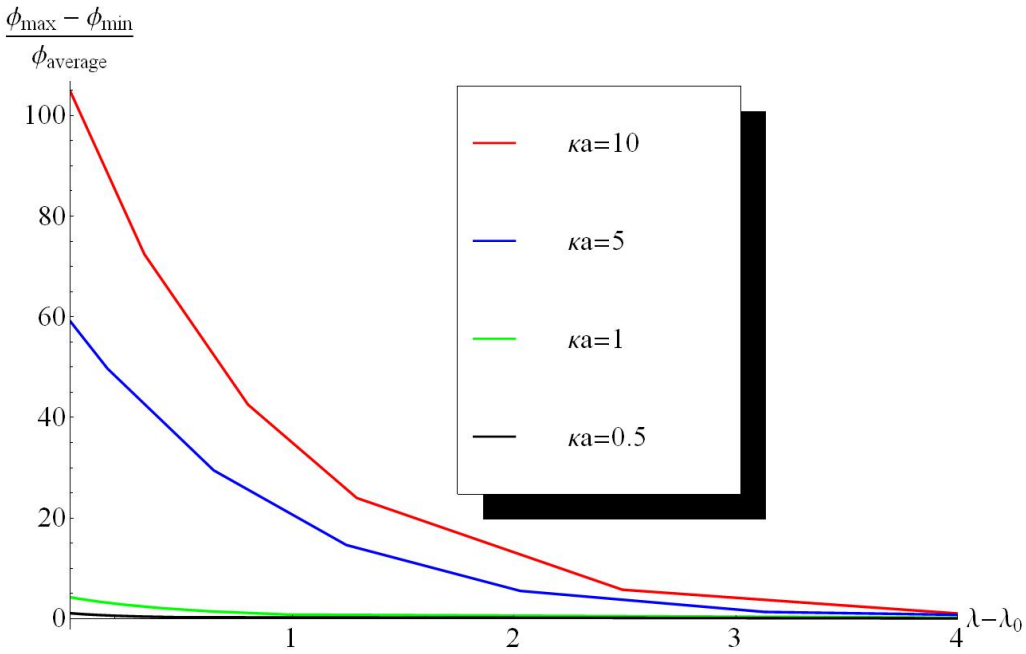

(a) Variation in potential for a colloid in an fcc lattice.

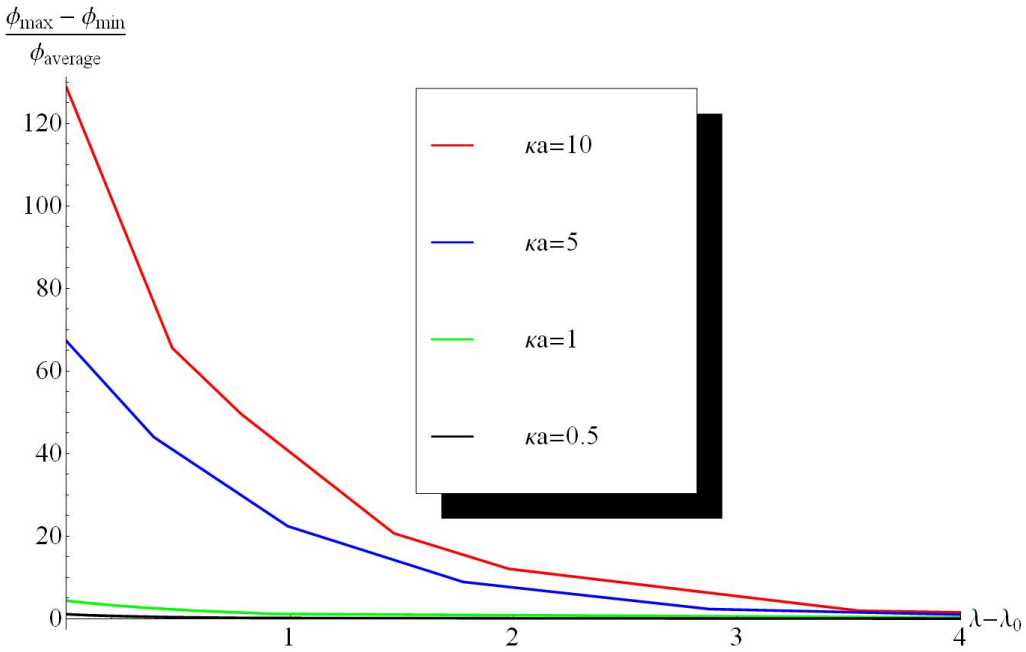

(b) Variation in potential for a colloid in a bcc lattice.

Figure 4.4: Variation in surface potential $\phi_{\text{max}}-\phi_{\text{min}}$ in percentage of the average surface potential ϕ_{average} for colloids with charge $Z\lambda_b/\kappa^2 a = 0.1$ in (a) an fcc and (b) a bcc crystal at various κa, as a function of $\lambda - \lambda_0$ as defined in Eq. (2.69) and below, i.e. such that $\lambda - \lambda_0 = 0$ corresponds to close packing.

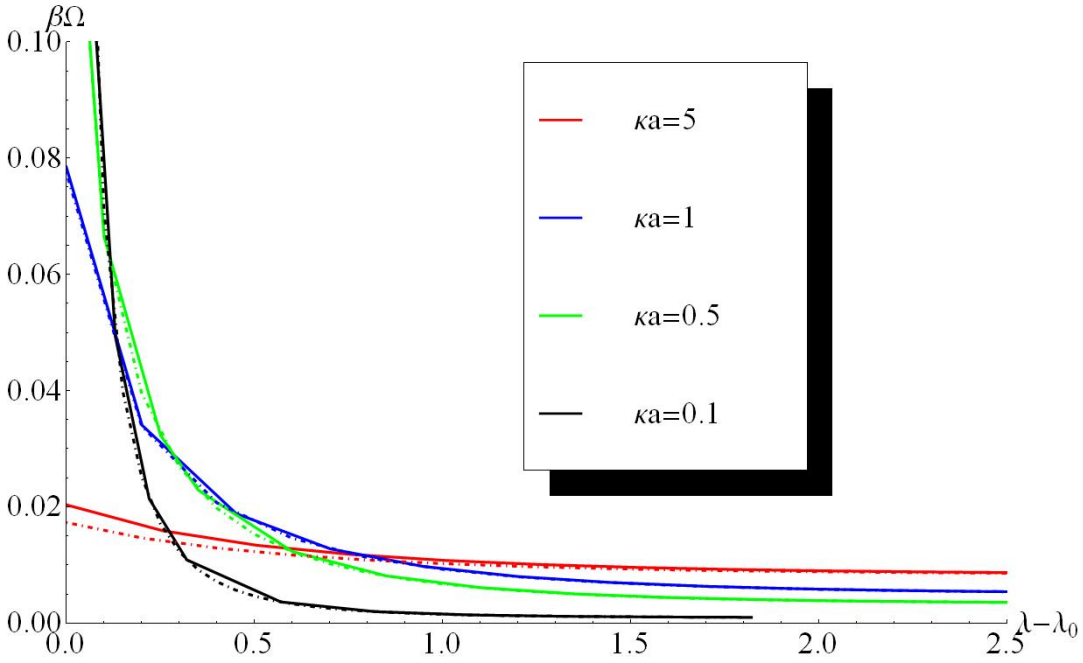

(a) Comparison between spherical approximation and an fcc WS cell.

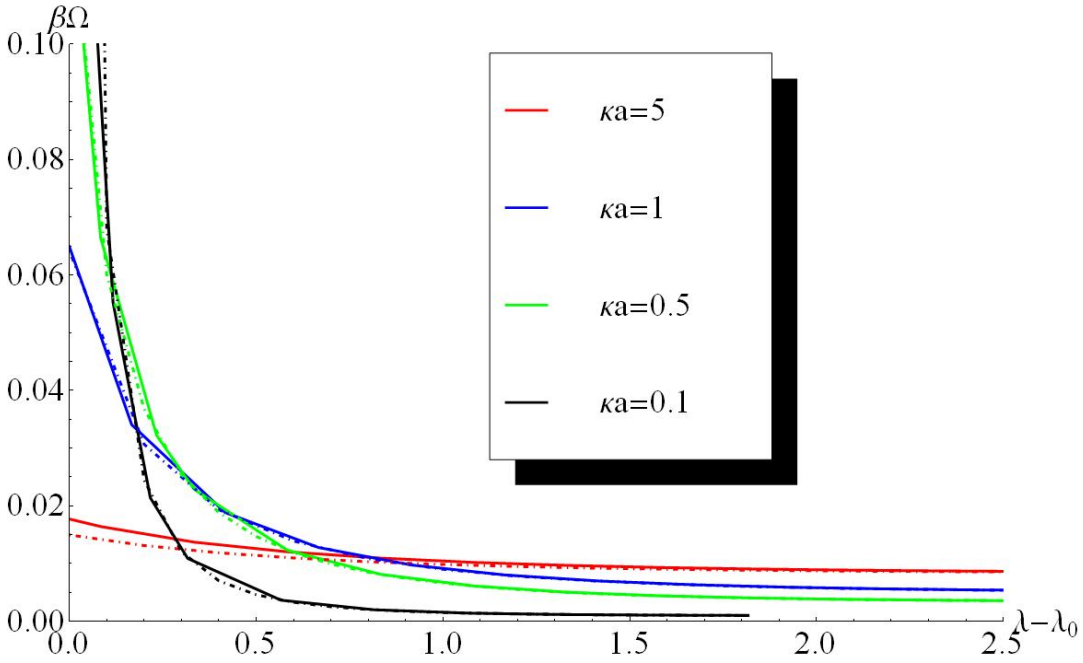

(b) Comparison between spherical approximation and a bcc WS cell.

Figure 4.5: Cell grand potential (Eq. (2.58)) in units of kT for colloids with charge $Z\lambda_b/\kappa^2 a = 0.1$ in a non-spherical (continuous lines) and spherical (dotted lines) WS cell (Eq. (2.59)), as a function of $\lambda - \lambda_0$ as defined in Eq. (2.69) and below, i.e. such that $\lambda - \lambda_0 = 0$ corresponds to close packing.

4.3 Comparison with DLVO theory

The grand potential of the cell in the WS model Ω_{WSC} (Eq. (2.58)) can also be expressed in units of the grand potential Ω_{DLVO} which DLVO-theory gives for the same system parameters by summing over the pair potential Eq. (2.45) multiplied with the renormalized charge $Ze^{\kappa a}/(1+\kappa a)$, see Fig. 4.6. From this figure it follows that in the interval $\lambda - \lambda_0 < 1$ DLVO-theory predicts a grand potential which is several times smaller than the grand potential of the system computed with the WS model. For low κa the difference between DLVO and the WS model is greater than for big κa. This effect has also been discussed in chapter 2 and is caused by overlap of the double layers of different colloids. This means that there is not a direct link with the heterogeneous zeta-potential of the colloids, in which big κa has a greater surface potential variation. The second thing to notice is that for all κa and in both the fcc and the bcc crystals in the low packing limit, $\lambda - \lambda_0 \to \infty$, the grand potential of DLVO-theory and WS theory become the same. This is in agreement with the theory in chapter 2. Because DLVO-theory is only valid when the colloids are far apart, i.e. ion distributions around each colloid are induced only by the colloid itself, not its neighbors, we must find that DLVO-theory is a good theory when the density is low.

4.3.1 fcc/bcc phase transition

When considering the grand potential difference between fcc and bcc crystal structures which are given by the WS cell model (Eq. (2.58)) it turns out that, because of the high precision one must obtain, it is not possible to determine the correct critical value λ_c as found in chapter 2. The reason why one cannot obtain the correct critical value is that the grand potential difference still depends heavily on the number of slices N of the interval on which one solves the PB-equation (see appendix B) and on the number of points one uses to compute the flux through the non-spherical geometric shape, although this dependence is much weaker. Because of the high precision one must have to correctly predict the critical value for the phase transition the number of slices seem to matter, but for the other results in this chapter this dependence can be neglected so those results are all valid and can be trusted. An interesting quantity to consider nonetheless is $1 - \Omega_{\text{DLVO}}/\Omega_{\text{WSC}}$, which is depicted on a logarithmic scale in Fig. 4.7 for three different number of slices with $\kappa a = 0.1$. From this figure the dependence on the number of slices is made clear. One observes that for larger cells a very high number of slices is necessary (so very small intervals to solve the PB-equation, see appendix B) to converge to a fixed value for the ratio $1 - \Omega_{\text{DLVO}}/\Omega_{\text{WSC}}$. Remarkable is the linear behavior this quantity seems to display for the low values of λ.

In Fig. 4.8 linear fits were made for three different values of κa for the values of

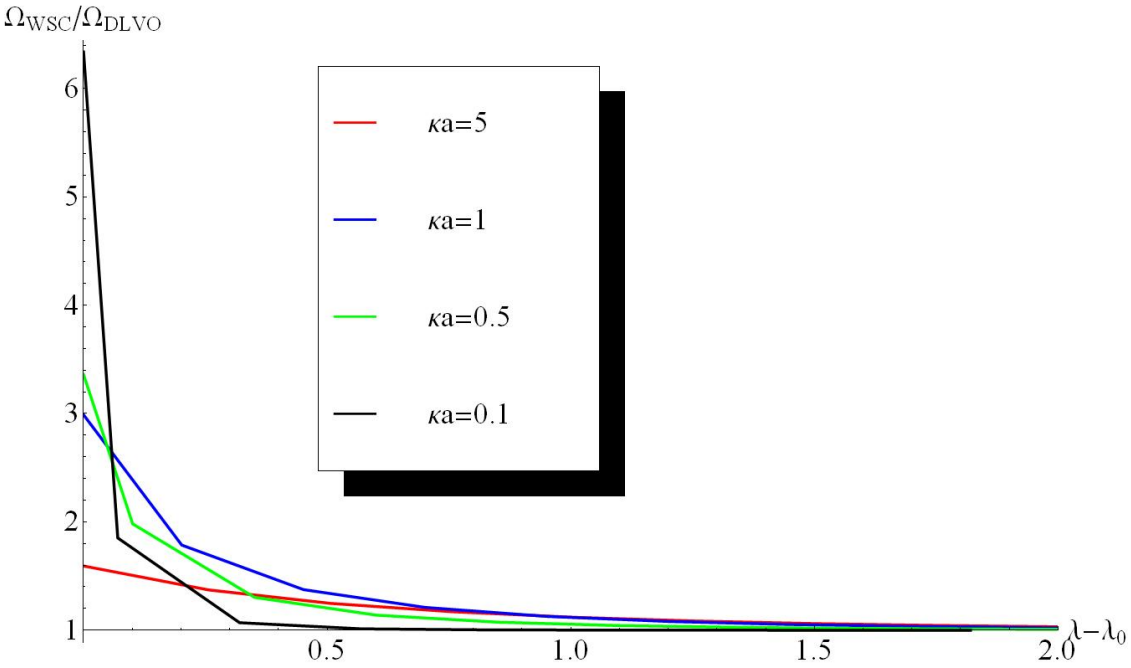

(a) Grand potential of an fcc WS cell in units of the grand-potential predicted by DLVO-theory.

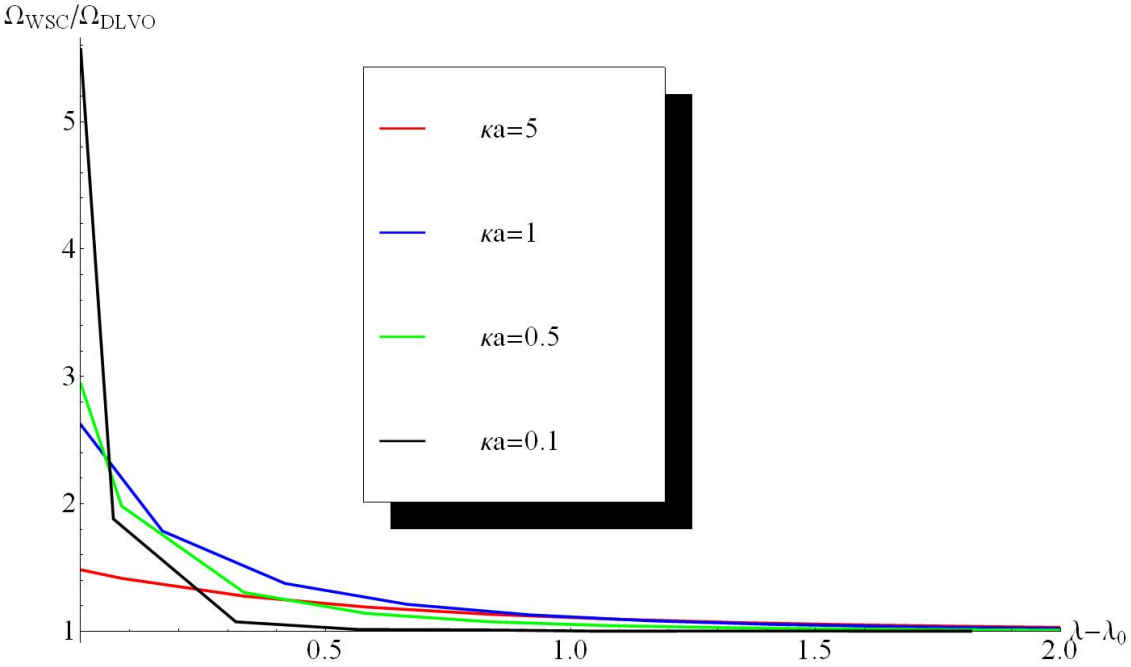

(b) Grand potential of a bcc WS cell in units of the grand-potential predicted by DLVO-theory.

Figure 4.6: Grand potential of the WS cell Ω_{WSC} (Eq. (2.58)) of an fcc and a bcc crystal in units of the corresponding grand potential Ω_{DLVO} predicted by DLVO-theory by summing over the pair potential in Eq. (2.45) multiplied with the renormalized charge $Ze^{\kappa a}/(1+\kappa a)$ for various κa, as a function of $\lambda - \lambda_0$ as defined in Eq. (2.69) and below, i.e. such that $\lambda - \lambda_0 = 0$ corresponds to close packing.

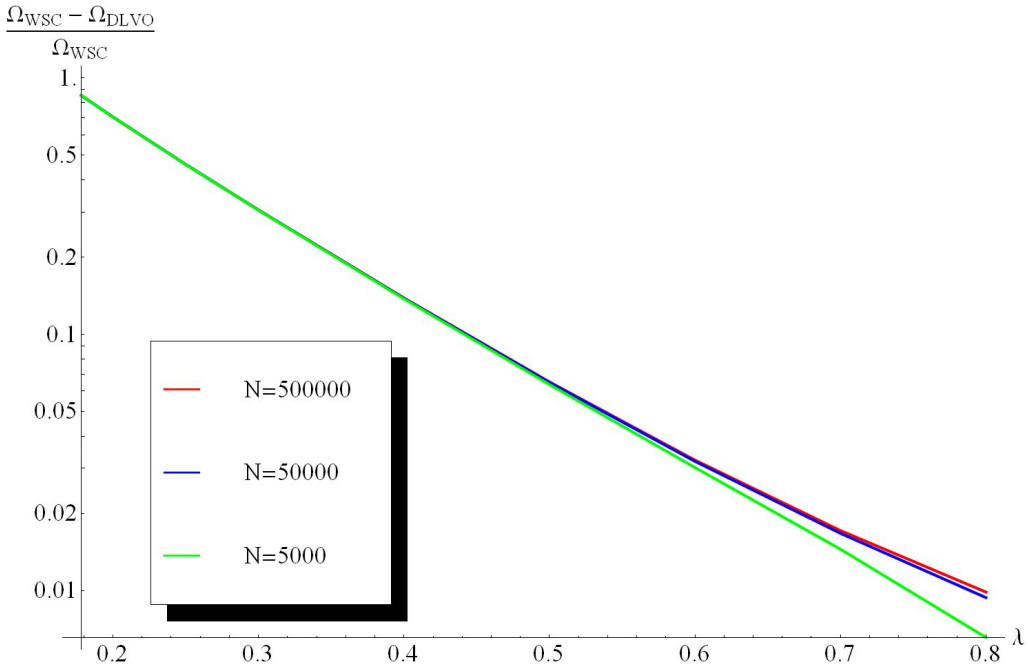

Figure 4.7: The ratio $1 - \Omega_{DLVO}/\Omega_{WSC}$ in a fcc crystal for $\kappa a = 0.1$ on a logarithmic scale plotted for three different values of the number of slices N used to solve the PB-equation, as a function of λ as defined in Eq. (2.69).

λ where $1 - \Omega_{DLVO}/\Omega_{WSC}$ varies linearly with λ. With these linear fits it becomes possible to express the grand potential found in our WS cell model (Eq. 2.58) in terms of the grand potential given by DLVO-theory, namely

$$\Omega_{WSC}(\lambda) = \frac{\Omega_{DLVO}(\lambda)}{1 - \exp(-\alpha\lambda + \beta)}, \tag{4.1}$$

with $-\alpha\lambda + \beta$ the linear equation used for the fit in Fig. 4.8.

Of course one can argue that the linear relation breaks down for higher λ and that eq. (4.1) is not valid in that regime. One should keep in mind, however, that from the previous section we know that DLVO-theory works well at lower densities and only gives rise to deviations at the higher densities. Equation (4.1) gives a high density correction for DLVO theory and converges for $\lambda \to \infty$ to regular DLVO-theory. In Fig. 4.9 the grand potential given by the "corrected" DLVO-theory is plotted together with the grand potential given by the WS cell model and the grand potential predicted by the regular DLVO-theory, and perfect agreement between the WS cell model and the "corrected" DLVO-theory as given by eq. (4.1) is observed. The results shown here are for the fcc case, the bcc case behaves itself in exactly the same manner.

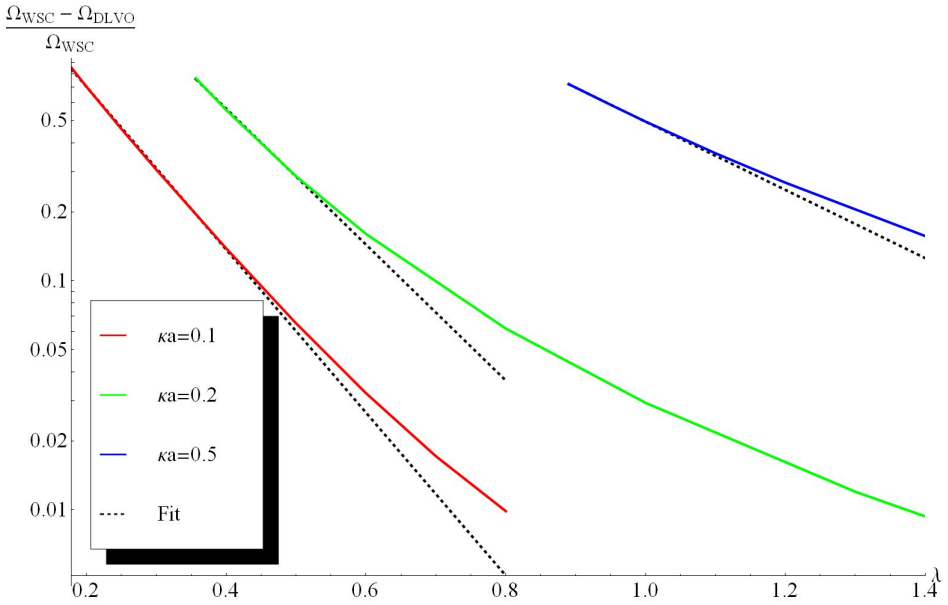

Figure 4.8: $1-\Omega_{\mathrm{DLVO}}/\Omega_{\mathrm{WSC}}$ in a fcc crystal for three different values of κa on a logarithmic scale together with their linear fits (dotted lines) as a function of λ as defined in Eq. (2.69).

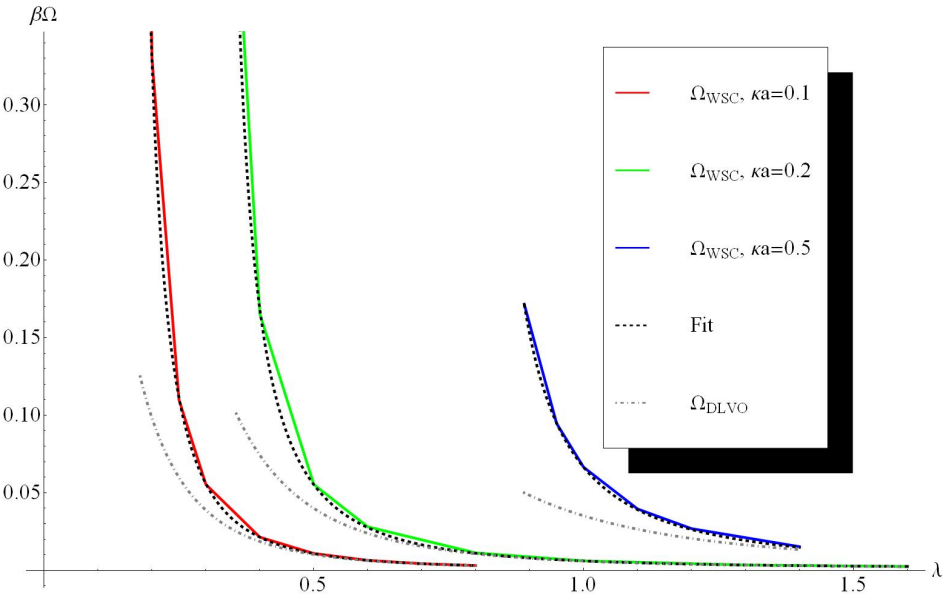

Figure 4.9: Grand potential of an fcc WS cell in the WS cell model, "corrected" DLVO theory (black) and normal DLVO theory (gray) for three values of κa as a function of λ as defined in Eq. (2.69).

Using this correction for DLVO-theory it becomes also possible to look at the phase transition between fcc and bcc crystals. In Fig. 4.10 the grand potential difference $\beta\Delta\Omega$ between bcc and fcc is plotted for three different values of κa. We observe that for $\kappa a = 0.1$ we get a critical value around the expected $\lambda_c \approx 1.74$ as found in chapter 2 and for higher values of κa this critical point disappears. There appear to be also additional critical values, for $\kappa a = 0.1$ at $\lambda \approx 0.37$ and $\lambda \approx 1.3$, for $\kappa a = 0.2$ at $\lambda \approx 0.49$ and for $\kappa a = 0.5$ at $\lambda \approx 1.05$. The transitions for $\kappa a = 0.2$ and $\kappa a = 0.5$ together with the transition of $\kappa a = 0.1$ at $\lambda \approx 0.37$ lie at the boundary of the linear regime in Fig. 4.8, which suggest that these phase transition are not physical, but caused by the use of the approximation eq. (4.1). The critical point for $\kappa a = 0.1$ at $\lambda \approx 1.3$ is most likely caused as a side effect of the additional numerical critical points, but more research is necessary to be conclusive about this. Because of the increase in grand-potential even far in the DLVO regime (Fig. 4.10) for higher κa we can conclude that the critical value $\lambda_c \approx 1.74$ as is found in chapter 2 for the point particle limit disappears when κa increases and so only a fcc phase exist in this case.

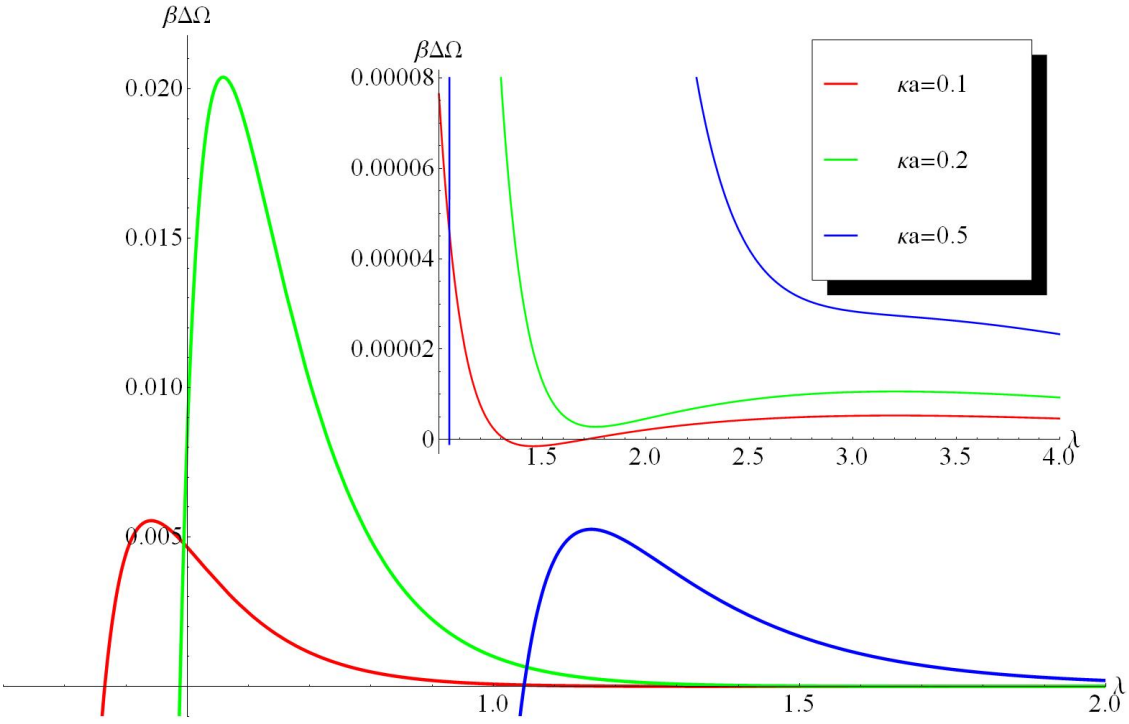

Figure 4.10: Grand potential difference $\beta\Delta\Omega = \beta(\Omega_{\text{bcc}} - \Omega_{\text{fcc}})$ between a bcc and a fcc crystal in the approximation (4.1) for three different κa values as a function of λ as defined in Eq. (2.69). The figure at the top right is a close-up on the interval $1 \leq \lambda \leq 4$.

4.4 Dielectric ratios

Finally we consider in Fig. 4.11 the effect of different dielectric ratios $\epsilon_r = \epsilon_{\text{colloid}}/\epsilon_{\text{solvent}}$ on the grand potential Eq. (2.58). From this figure it follows that for $\kappa a \leq 1$ there is no difference between the different dielectric ratios. Only when considering larger values of κa one observes a small effect at high densities. At these high densities one sees that a lower ratio leads to a higher grand potential. The reason why only at high κa there is an effect is because for spherical WS cells, Eq. (2.59), different dielectric ratios all give the same result, in accordance with the boundary problem as defined in chapter 3. As we discussed above, for $\kappa a \leq 1$ the variation in surface potential is not significant enough to give a grand potential that is very different than the one in the spherical approximation. This means that only when the spherical WS cell approximation is no longer valid it becomes possible to have a grand potential difference for different dielectric ratios between colloid and solvent and this only happens when $\kappa a > 1$.

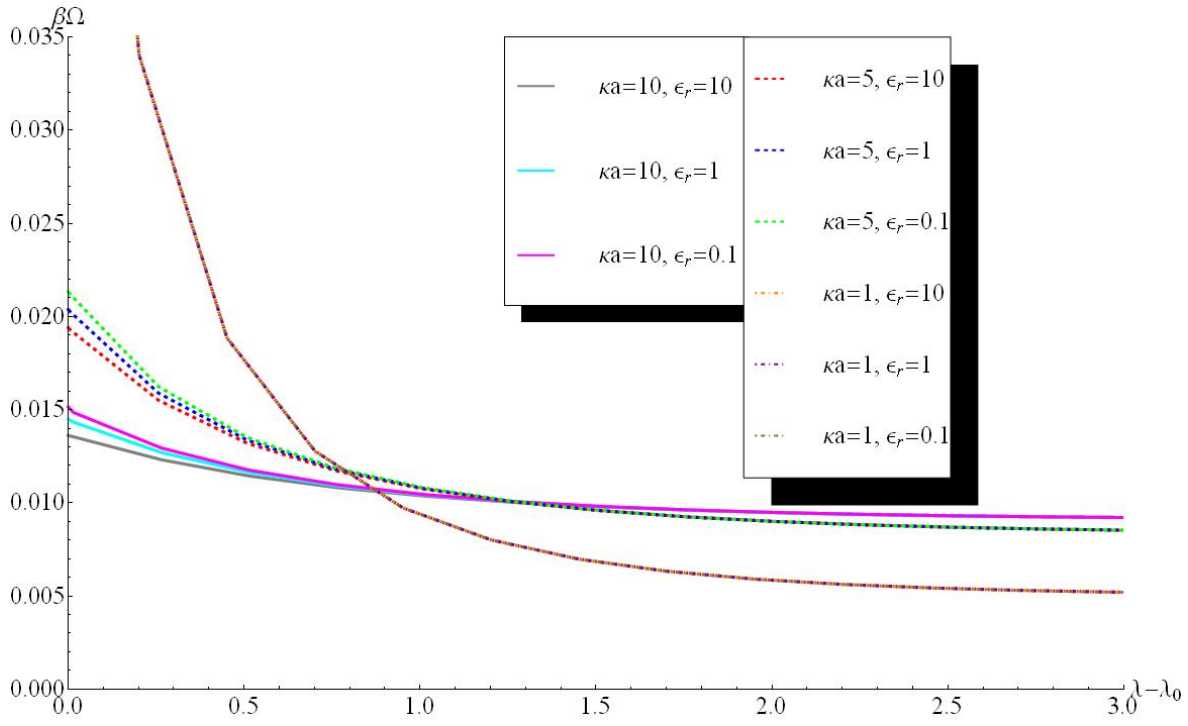

(a) fcc crystal.

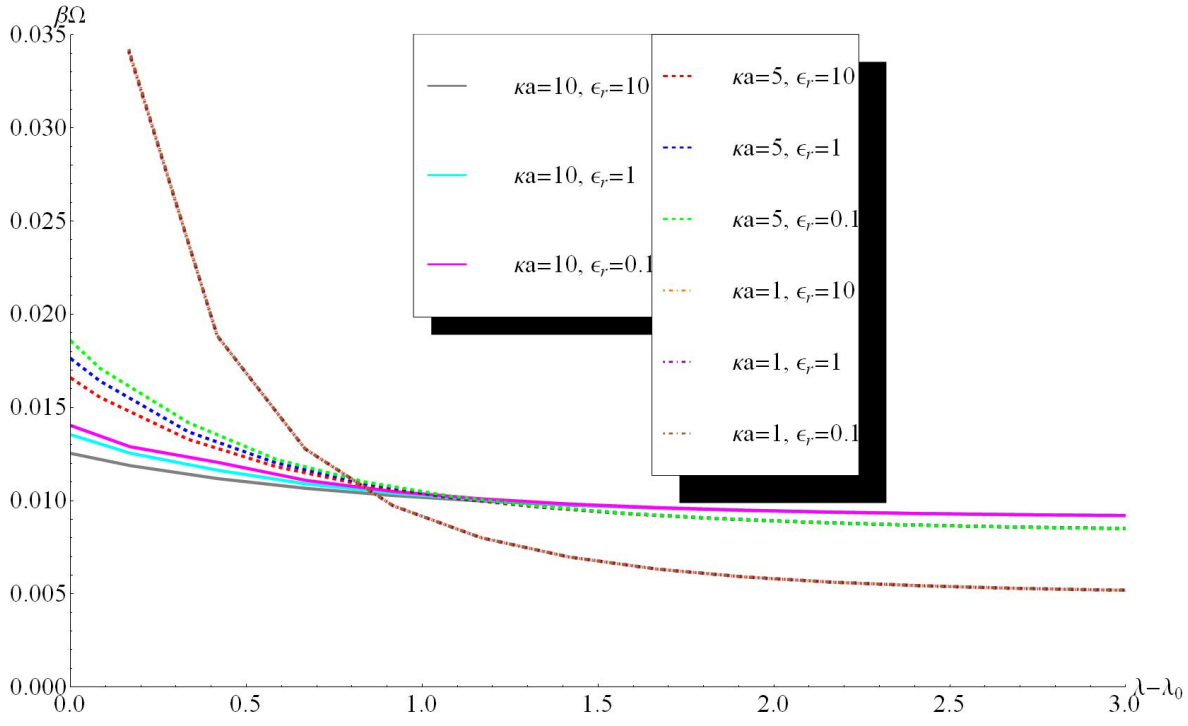

(b) bcc crystal.

Figure 4.11: Grand potential of a WS cell (Eq. (2.58)) for colloids with charge $Z\lambda_b/\kappa^2 a = 0.1$ for various κa and dielectric ratios ϵ_r, as a function of $\lambda - \lambda_0$ as defined in Eq. (2.69) and below, i.e. such that $\lambda - \lambda_0 = 0$ corresponds to close packing.

4.5 Conclusion

From the numerical results we can conclude that the method for treating non-spherical Wigner-Seitz cells as presented in chapter 3 leads to good results for linear Poisson-Boltzmann theory. The low density behavior was as expected and at high densities the effect of overlapping double layers becomes clear. Especially for $\kappa a > 1$ we see that the inhomogeneity of the potential distribution on the colloid's surfaces become significant and this implies that the spherical approximation as introduced by Ref. [9] is no longer valid. DLVO-theory also breaks down at higher densities and a correction term for this theory becomes necessary. It should be mentioned, however, that the original DLVO-theory was derived for only two particles. The modern application of this theory uses it in many-colloid systems, so perfect agreement with the non-spherical Wigner-Seitz cell model was not expected. The conclusion one should have about DLVO-theory in this sense is that the theory is only valid for the systems it was derived from and caution should be paid when applying it to much more complex systems such as colloid crystals. Finally we observed that the fcc and bcc crystal structures are not very different from each other as regards the surface potential distribution. In almost all numerical results the two structures behaved very similar. This is also the cause for the very small grand-potential difference between them at low densities, which makes it very hard to find the "$T = 0$" phase transition. The main point of improvement of our method is to try to find minimizing schemes that are more precise, especially when one wants to apply this method to non-linear Poisson-Boltzmann theory.

Bibliography

[1] N. Boon. *Electrostatics in ionic solution - work and energy, charge regulation, and inhomogeneous surfaces*. PhD thesis, Universiteit Utrecht, 2012. [cited at p. 1, 3, 5, 16, 19]

[2] L. Li. Colloidal crystal: emergence of long range order from colloidal fluid. Emergent States of Matter course essay - University of Illinois, December 2008. [cited at p. 2]

[3] B. Zoetekouw. *Phase behavior of charged colloids many-body effects, charge renormalization and charge regulation*. PhD thesis, Universiteit Utrecht, 2006. [cited at p. 2, 3, 5, 11, 19, 23, 24, 64]

[4] J. Drelich and Y. U. Wang. Charge heterogeneity of surfaces: Mapping and effects on surface forces. *Advances in Colloid and Interface Science*, pages 91–101, January 2011. Presented during the XIVth International Conference on Surface Forces, Moscow-St. Petersburg, Russia, June 21 till June 27, 2010. [cited at p. 2, 3]

[5] R. van Roij. soft condensed matter theory - lecture notes, 2007-2008. Notes for Soft Condensed Matter Theory course - Universiteit Utrecht. [cited at p. 5, 9]

[6] G. Kahl and H. Löwen. Classical density functional theory: an ideal tool to study heterogeneous crystal nucleation. *J. Phys.: Condens. Matter 21 464101*, pages 1–2, 2009. [cited at p. 9]

[7] M. Deserno and H. H. von Grünberg. The osmotic pressure of charged colloidal suspensions: A unified approach to linearized poisson-boltzmann theory. *Phys. Rev. E66 011401*, 2002. [cited at p. 14]

[8] N. Boon. Screening effects and charge in suspensions of colloidal spheres. Master's thesis, Universiteit Utrecht, 2008. [cited at p. 17, 18]

[9] S. Alexander, P. M. Chaikin, P. Grant, G. Morales, P. Pincus, and D. Hone. Charge renormalization, osmotic pressure, and bulk modulus of colloidal crystals: Theory. *J. Chem. Phys. 80, 5776*, 1984. [cited at p. 21, 49]

[10] J.R. Hook and H.E. Hall. *Solid State Physics*. John Wiley & sons, second edition, 1991. [cited at p. 23, 24]

[11] K. Kremer, M. O. Robbins, and G. S. Grest. Phase diagram of yukawa systems: Model for charge-stabilized colloids. *Phys. Rev. Let. 57, 21*, 1986. [cited at p. 27]

[12] V. L. Colvin. From opals to optics: colloidal photonic crystals. *MRS Bulletin*, pages 631–641, August 2001. [cited at p. 31]

[13] M.I.A. Lourakis. levmar: Levenberg-marquardt nonlinear least squares algorithms in C/C++. [web page] http://www.ics.forth.gr/ lourakis/levmar/, Jul. 2004. [Accessed on 31 Jan. 2005.]. [cited at p. 60]

Appendices

Appendix A

Spherical Harmonics

Spherical harmonics arise when considering Laplace's equation for an electric potential $V(\mathbf{r})$ in spherical coordinates $\mathbf{r} = (r, \theta, \phi)$*, i.e.

$$\nabla^2 V(\mathbf{r}) = \frac{1}{r^2}\frac{\partial}{\partial r}\Big(r^2\frac{\partial V}{\partial r}\Big) + \frac{1}{r^2\sin\theta}\frac{\partial}{\partial\theta}\Big(\sin\theta\frac{\partial V}{\partial\theta}\Big) + \frac{1}{r^2\sin^2\theta}\frac{\partial^2 V}{\partial\phi^2} = 0. \quad \text{(A.1)}$$

Applying a separation of variables $V(\mathbf{r}) = R(r)Y(\theta,\phi)$ leads to the following equation

$$\frac{1}{R}\frac{d}{dr}\Big(r^2\frac{dR}{dr}\Big) = -\frac{1}{Y\sin\theta}\frac{\partial}{\partial\theta}\Big(\sin\theta\frac{\partial Y}{\partial\theta}\Big) - \frac{1}{\sin^2\theta}\frac{\partial^2 Y}{\partial\phi^2}. \quad \text{(A.2)}$$

Since the left side only depends on r and the right side depends only on (θ,ϕ), both sides must be constant. Introducing the separation constant $l(l+1)$ leads to the following set of equations

$$\begin{aligned} \frac{1}{R}\frac{d}{dr}\Big(r^2\frac{dR}{dr}\Big) &= l(l+1) \\ \sin\theta\frac{\partial}{\partial\theta}\Big(\sin\theta\frac{\partial Y}{\partial\theta}\Big) + \frac{\partial^2 Y}{\partial\phi^2} &= -\,l(l+1)\sin^2\theta Y. \end{aligned} \quad \text{(A.3)}$$

The radial equation has as a solution

$$R(r) = Ar^l + \frac{B}{r^{l+1}}, \quad \text{(A.4)}$$

with A and B two integration constants.

*Actually, spherical harmonics arise in many physical problems, be it either classical or quantum mechanical, such as the solution of the Schrodinger equation in spherical coordinates, atomic electron configurations and, of course, in electrostatics. Also, spherical harmonics have applications in the field of computer graphics by their applicability to light transport.

The angular part is harder to solve and the solution to this equation will give us the spherical harmonics. To proceed, again do a separation of variables $Y(\theta,\phi) = \Theta(\theta)\Phi(\phi)$ and introduce a separation constant m^2. This again leads to a set of equations,

$$\frac{1}{\Theta}\left[\sin\theta\frac{d}{d\theta}\Big(\sin\theta\frac{d\Theta}{d\theta}\Big)\right] + l(l+1)\sin^2\theta = m^2 \tag{A.5}$$

$$\frac{1}{\Phi}\frac{d^2\Phi}{d\phi^2} = -m^2. \tag{A.6}$$

Equation (A.6) can be easily be solved and has as a solution† $\Phi(\phi) = e^{im\phi}$. By rotating in space over an angle of 2π we return to the same point, so it should be required that $\Phi(\phi + 2\pi) = \Phi(\phi)$. This leads to the conclusion that m needs to be an integer, so at this moment we have $m = 0, \pm1, \pm2, ...$ To solve equation (A.5), define the lth Legendre polynomial $P_l(x)$ by the Rodrigues formula

$$P^l(x) \equiv \frac{1}{2^l l!}\Big(\frac{d}{dx}\Big)^l (x^2-1)^l. \tag{A.7}$$

Now the associated Legendre polynomial is defined by

$$P^l_m(x) \equiv (1-x^2)^{|m|/2}\Big(\frac{d}{dx}\Big)^{|m|} P^l(x), \tag{A.8}$$

which gives the solution to (A.5), $\Theta(\theta) = CP^l_m(\cos\theta)$, with C an integration constant. From the definition of the associated Legendre polynomial it follows that if $|m| > l$, then $P^l_m(x) = 0$, since the lth Legendre polynomial is a polynomial of degree l. All that needs to be done now is to normalize the spherical harmonic function $Y^l_m(\theta,\phi) = CP^l_m(\cos\theta)e^{im\phi}$, i.e. choose C is such a way that $\int_0^{2\pi} d\phi \int_0^{\pi} d\theta \sin\theta Y^l_m(\theta,\phi)^* Y^l_m(\theta,\phi) = 1$, where the star denotes complex conjugation. Working this out gives the following general expression for the spherical harmonics

$$Y^l_m(\theta,\phi) = \epsilon\sqrt{\frac{(2l+1)}{4\pi}\frac{(l-|m|)!}{|(l+|m|)!}}e^{im\phi}P^l_m(\cos\theta), \tag{A.9}$$

where $\epsilon = (-1)^m$ if $m \geq 0$ and $\epsilon = 1$ if $m < 0$. The first few spherical harmonics are listed in table A.1.

We will now discuss some useful properties of spherical harmonics. The first property follows from (A.3), which implies that the spherical harmonics are eigenfunctions

†It is usual in electrostatics to work with cosine and sine, instead of complex exponential, by the reality condition of the potential function. Since we are solving here the general Laplace's equation, there is no problem working with complex numbers and it also makes the calculations more easy. When doing numerical calculations, however, it is more appropriate to work with the real solutions.

Table A.1: The first few spherical harmonics $Y_m^l(\theta,\phi)$ in complex form.

$Y_0^0 = \left(\frac{1}{4\pi}\right)^{1/2}$	$Y_{\pm 2}^2 = \left(\frac{15}{32\pi}\right) \sin^2\theta e^{\pm 2i\phi}$
$Y_0^1 = \left(\frac{3}{4\pi}\right)^{1/2} \cos\theta$	$Y_0^3 = \left(\frac{7}{16\pi}\right)^{1/2} (5\cos^3\theta - 3\cos\theta)$
$Y_{\pm 1}^1 = \mp\left(\frac{3}{8\pi}\right)^{1/2} \sin\theta e^{\pm i\phi}$	$Y_{\pm 1}^3 = \mp\left(\frac{21}{64\pi}\right)^{1/2} \sin\theta(5\cos^2\theta - 1)e^{\pm i\phi}$
$Y_0^2 = \left(\frac{5}{16\pi}\right)^{1/2} (3\cos^2\theta - 1)$	$Y_{\pm 2}^3 = \left(\frac{105}{32\pi}\right)^{1/2} \sin^2\theta\cos\theta e^{\pm 2i\phi}$
$Y_{\pm 1}^2 = \mp\left(\frac{15}{8\pi}\right)^{1/2} \sin\theta\cos\theta e^{\pm i\phi}$	$Y_{\pm 3}^3 = \mp\left(\frac{35}{64\pi}\right)^{1/2} \sin^3\theta e^{\pm 3i\phi}$

of the Laplace operator, $r^2\nabla^2 Y_m^l(\theta,\phi) = -l(l+1)Y_m^l(\theta,\phi)$. Secondly, they are orthogonal,

$$\int_0^{2\pi} d\phi \int_0^{\pi} d\theta \sin\theta Y_m^l(\theta,\phi) Y_{m'}^{l'}(\theta,\phi) = \delta_{l,l'}\delta_{m,m'}, \tag{A.10}$$

with $\delta_{x,y}$ the Kronecker delta which is one when $x = y$ and zero in all other cases. From the definition of the associated Legendre polynomials, it also follows that, if $m > 0$, $Y_{-m}^l = (-1)^m (Y_m^l)^*$. The final property we mention here is that the spherical harmonics form a complete orthonormal basis for the space of square-integrable functions on the unit sphere. This means that any square-integrable function $f(\theta,\phi)$ on the unit sphere can be expanded in terms of spherical harmonics

$$f(\theta,\phi) = \sum_{l=0}^{\infty} \sum_{m=-l}^{l} f_m^l Y_m^l(\theta,\phi), \tag{A.11}$$

where the coefficients f_m^l are determined by the projection

$$f_m^l = \int_0^{2\pi} d\phi \int_0^{\pi} d\theta \sin\theta f(\theta,\phi) Y_m^l(\theta,\phi)^*. \tag{A.12}$$

Appendix B

Numerical methods

B.1 Euler and Newton method

If given is a second-order differential equation $f''(x) = F(f(x), f'(x), x)$ with boundary conditions $f'(a) = f_a$ and $f'(b) = f_b$ $(b > a)$, where $F(f(x), f'(x), x)$ an arbitrary function, a good numerical method to compute the solution to this differential equation is the Euler method. Start off by dividing the interval $[a, b]$ in $N+1$ intervals $[x_i, x_{i+1}]$, with $x_0 = a$ and $x_N = b$, which can be either of equal size or of varying size. The main idea is that on each segment the function $f(x)$ and $f'(x)$ are linear. This means that if we take a starting value $f(a) = f_0$ the value of f at x_1 can be computed by

$$\begin{aligned} f(x_1) &= f(a) + \frac{b-a}{N} f'(a) = f(a) + \frac{b-a}{N} f_a \\ f'(x_1) &= f'(a) + \frac{b-a}{N} f''(a) = f'(a) + \frac{b-a}{N} F(f(a), f'(a), a). \end{aligned} \tag{B.1}$$

This process can be repeated until one reaches the point $x_N = b$. Now a value $\tilde{f}'(b) = \tilde{f}_b$ is found, which of course still depends on the chosen start value f_0. In general $\tilde{f}_b \neq f_b$, so a second numerical trick must be employed, this will be the Newton method. The Newton method is a recipe for finding the root of a function $g(x)$. The idea is to linearize $g(x)$ in a point c_0 which is guessed to be a root and calculate the root c_1 of the obtained linear function. The claim is that c_1 is a better guess than c_0. Applying the same trick again leads to an even better guess and should, under reasonable assumptions, converge to the real root of the function. An explicit expression for finding the next guess is found by considering the root of the

linear approximation of $g(x)$,

$$g'(c_i) = \frac{g(c_i) - 0}{c_i - c_{i+1}}$$
$$\Rightarrow c_{i+1} = c_i - \frac{g(c_i)}{g'(c_i)}. \tag{B.2}$$

To apply this scheme to the Euler method means we must find the root of an appropriate constructed function. The function to take is $g(f_0) = \tilde{f}_b(f_0) - f_b$. For well-behaving differential equations the derivative of g is readily obtained by considering a solution for a slightly shifted starting value, i.e. $g(f_0 + \delta)$, with $\delta \ll 1$ and computing the following ratio leads to the derivative

$$g'(f_0) = \frac{g(f_0 + \delta) - g(f_0)}{\delta}. \tag{B.3}$$

By using the Newton method one obtains a series of starting values $f_0, f_1, f_2, ...$ which converges to the solution of the differential equation. Some care should always be taken, since for highly divergent or varying functions it is difficult to compute reliable derivatives in the Euler as well the Newton method and this can lead to wrong solutions.

B.2 Levenberg-Marquardt algorithm

The Levenberg-Marquardt algorithm is an ideal way to locate the minimum of a multivariate function that is expressed as the sum of squares of (non-)linear real valued functions. The discussion here is based on Ref. [13]. Let f be a function that maps a m-dimensional real parameter vector $\mathbf{p}$ to a n-dimensional ($n \geq m$) measurement vector $\hat{\mathbf{x}} = f(\mathbf{p})$. Now let a starting parameter-set $\mathbf{p}_0$ be given, together with a measured vector $\mathbf{x}$. The objective is to find a vector $\mathbf{p}^+$ that minimizes the squared distance $\epsilon^T \epsilon$, with $\epsilon = \mathbf{x} - \hat{\mathbf{x}}$ and T denoting vector transposition. To obtain this $\mathbf{p}^+$, start off by considering a linear approximation of f in a small neighborhood around $\mathbf{p}$. Let $\delta_\mathbf{p}$ be a m-dimensional vector with a small norm $\|\delta_\mathbf{p}\| \ll 1$, so that we obtain the following approximation,

$$f(\mathbf{p} + \delta_\mathbf{p}) \approx f(\mathbf{p}) + \mathbf{J}\delta_\mathbf{p}, \tag{B.4}$$

where $\mathbf{J} = \frac{\partial f(\mathbf{p})}{\partial \mathbf{p}}$ is the Jacobian of f. By the iterative nature of the optimization process, the quantity $\|\mathbf{x} - f(\mathbf{p} + \delta_\mathbf{p})\| \approx \|\mathbf{x} - f(\mathbf{p}) - \mathbf{J}\delta_\mathbf{p}\| = \|\epsilon - \mathbf{J}\delta_\mathbf{p}\|$ has to minimized at each iteration step and leads to a new value for $\mathbf{p}$, so one obtains a sequence $\mathbf{p}_0, \mathbf{p}_1, \mathbf{p}_2, ...$, which converges to $\mathbf{p}^+$ if the problem is not ill posed. The minimum of $\|\epsilon - \mathbf{J}\delta_\mathbf{p}\|$ is obtained when $\mathbf{J}\delta_\mathbf{p} - \epsilon$ is orthogonal to the column space of J, see Ref. [13], that is

$$\mathbf{J}^T(\mathbf{J}\delta_\mathbf{p} - \epsilon) = \mathbf{0}$$
$$\Rightarrow \mathbf{J}^T\mathbf{J}\delta_\mathbf{p} = \mathbf{J}^T\epsilon. \tag{B.5}$$

The contributions that Levenberg and Marquardt made to this optimizing method is to introduce a damping term $\mu > 0$ and a matrix $\mathbf{N}$, where the off diagonal elements of $\mathbf{N}$ are the same as in $\mathbf{J}^T\mathbf{J}$ and the diagonal elements are given by $\mathbf{N}_{ii} = \mu + [\mathbf{J}^T\mathbf{J}]_{ii}$. The equation (B.5) is replaced by

$$\mathbf{N}\delta_{\mathbf{p}} = \mathbf{J}^T\epsilon. \tag{B.6}$$

When a new value of $\mathbf{p}$ is calculated, one checks that this reduces the error ϵ, if not, the damping term is multiplied by a scaling factor $\mu_s > 1$ and one computes again. This process continues until a decrease of the error is obtained and counts as a single Levenberg-Marquardt iteration. To also allow a decrease of the damping term at each calculation for a particular damping term μ, one also computes the error with the damping μ/μ_s. If the error of the latter is smaller than that of the former, one sets the damping to μ/μ_s. When the damping term is big, the Levenberg-Marquardt behaves itself as a steepest-decent method, and while when the damping is small it becomes more like the Gauss-Newton method. In this way the method allows fast navigation through parameter space when the value of $\mathbf{p}$ is very off and when around $\mathbf{p}^+$ the precision increases. To apply this method to the material discussed in chapter 3, one takes for the parameter $\mathbf{p}$ the constants c_m^l and for the function f the flux of the electric field through the surface of the WS cell under consideration.

List of Symbols and Abbreviations

Abbreviation	Description	Definition
e	elementary charge	
k_B	Boltzmann's constant	
β	inverse thermal energy	$\beta = \frac{1}{k_B T}$
λ_B	Bjerrum length	$\frac{e^2}{\epsilon k_B T}$
κ^{-1}	Debye length	$\kappa = \sqrt{8\pi\lambda_B \rho_s}$
PB-equation	Poisson-Boltzmann equation	
WS cell	Wigner-Seitz cell	

List of Figures